

PNNL-38364

Control Oriented Models for Co-Design

Technical Overview of MT-HVDC, MVDC, and Solid-State Transformer Building Blocks

September 2025

Hisham Mahmood Buxin She Gian Paramo Roshan L. Kini Priya T. Mana Marcelo A. Elizondo



DISCLAIMER

This report was prepared as an account of work sponsored by an agency of the United States Government. Neither the United States Government nor any agency thereof, nor Battelle Memorial Institute, nor any of their employees, makes any warranty, express or implied, or assumes any legal liability or responsibility for the accuracy, completeness, or usefulness of any information, apparatus, product, or process disclosed, or represents that its use would not infringe privately owned rights. Reference herein to any specific commercial product, process, or service by trade name, trademark, manufacturer, or otherwise does not necessarily constitute or imply its endorsement, recommendation, or favoring by the United States Government or any agency thereof, or Battelle Memorial Institute. The views and opinions of authors expressed herein do not necessarily state or reflect those of the United States Government or any agency thereof.

PACIFIC NORTHWEST NATIONAL LABORATORY

operated by

BATTELLE

for the

UNITED STATES DEPARTMENT OF ENERGY

under Contract DE-AC05-76RL01830

Printed in the United States of America

Available to DOE and DOE contractors from the Office of Scientific and Technical Information, P.O. Box 62, Oak Ridge, TN 37831-0062

ph: (865) 576-8401 fox: (865) 576-5728 email: reports@osti.gov

Available to the public from the National Technical Information Service 5301 Shawnee Rd., Alexandria, VA 22312 ph: (800) 553-NTIS (6847) or (703) 605-6000

email: info@ntis.gov
Online ordering: http://www.ntis.gov

Control Oriented Models for Co-Design

Technical Overview of MT-HVDC, MVDC, and Solid-State Transformer Building Blocks

September 2025

Hisham Mahmood Buxin She Gian Paramo Roshan L. Kini Priya T. Mana Marcelo A. Elizondo

Prepared for the U.S. Department of Energy under Contract DE-AC05-76RL01830

Pacific Northwest National Laboratory Richland, Washington 99354

Abstract

The electric power system is shifting toward a power-electronics—enabled grid, where converter-based "building blocks" (e.g., high-voltage direct current (HVDC) links, multi-terminal HVDC (MT-HVDC) networks, medium-voltage DC (MVDC) links, and solid-state transformers (SSTs)) provide fast, precise control of power flows, voltage, and frequency. This report develops and applies publicly shareable electromagnetic transient (EMT) and phasor models to examine how such building blocks can be composed and coordinated to support offshore wind integration, inter-area transfers, feeder support, and resilience.

Section 2 documents a modular multilevel converter (MMC)—based MT-HVDC modeling framework and two use cases: a compact WSCC/IEEE 9-bus test system and a 240-bus "mini-WECC" case with five offshore wind plants (OWFs). Phasor-to-EMT transfer, initialization, and sanity checks are summarized, and neutral demonstrations of normal and contingency operation are reported. Section 3 frames the problem of wind-plant inertial frequency response (IFR): shaping energy release and recovery to improve nadir while avoiding aerodynamic stall; representative simulations illustrate the issues without disclosing proprietary control. Section 4 develops MVDC concepts through an IEEE 16-bus loop and an Olympic Peninsula case study that compares AC vs. MVDC corridors and shows how feeder headroom can be pooled via DC couplers. Section 5 surveys SST architectures and identifies a gap: scalable, communication-free coordination of multiple SSTs for islanded feeder networks. Across the report, novel methods and configurations under separate publication and IP review are not disclosed; only topic-oriented, replicable setups and non-proprietary results are shown.

These models and use cases are intended as foundations for future publications and co-design studies on architecture, control, and coordination of PE-enabled grids.

Abstract

Summary

This public final report consolidates models, use-cases, and topic-focused studies developed under the umbrella **Power-Electronics–Enabled Grid Building Blocks**. The work targets how power-electronic (PE) assets—HVDC/MT-HVDC terminals, MVDC links, and solid-state transformers (SSTs)—can be composed and controlled to improve transfer capability, operability, and resilience as the grid decarbonizes. The report is deliberately **topic-oriented and non-proprietary**: it documents baseline architectures, models, and neutral studies that enable independent replication, while reserving novel control concepts and configurations for peer-reviewed publications and intellectual-property evaluation.

MT-HVDC modeling and use cases. We developed EMT-grade models and use-cases to examine multi-terminal HVDC (MT-HVDC) with modular multilevel converters (MMCs). A compact WSCC/IEEE 9-bus testbed in MATLAB/Simulink (Specialized Power Systems) supports rapid proof-of-concept studies with both detailed switching and averaged MMC variants. A larger EMT case in PSCAD was built by transferring the reduced 240-bus mini-WECC phasor model using E-Tran, completing converter and OWF modules, and initializing AC/DC states for fast-dynamic studies. Frequency-response comparisons versus the phasor case confirm consistency over the electromechanical band. Neutral operating scenarios (normal and contingency) illustrate DC-voltage regulation, power scheduling, and AC-side behavior without revealing new control methods.

Wind plants and inertial frequency response (IFR). Using the above testbeds, we frame the IFR problem for grid-connected wind plants: extracting kinetic energy during a frequency dip improves nadir but can induce (i) excessive rotor-speed depression (aerodynamic stall risk) and (ii) aggressive energy recovery that produces a secondary frequency dip. Illustrative simulations show conventional and "smooth-recovery" IFR responses and highlight the trade-space, without disclosing proprietary detection/mitigation strategies. The material supports safe discussion of benefits/risks and motivates separate, detailed publications.

MVDC links and meshed MVDC. We outline roles for MVDC in distribution and sub-transmission—corridor capacity increases, controllable power exchange, and routing flexibility—then exercise a three-terminal MVDC loop on an IEEE-16-bus-derived network. Studies demonstrate DC-slack assignment (single-slack vs. droop), scheduled inter-area transfers, and autonomous reassignment under simple contingencies. A second use-case compares AC versus MVDC corridors around Washington State's Olympic Peninsula. Results (steady-state capacity and high-level cost trends) show how smaller MVDC structures and rights-of-way can materially shift economics, while dynamic/protection topics remain out of scope for this public report.

Solid-state transformers (SSTs). We survey SST architectures (multi-stage AC/DC–DC/DC–DC/AC with high-frequency isolation; MMC-HF and DAB-based variants), grid services at MV/LV boundaries, and the state of prototypes. The literature is synthesized to identify a system-level gap: most work optimizes a **single** SST, whereas feeder-level coordination of **multiple** SSTs—especially under islanded operation—remains underexplored. This gap frames the motivation for separate, non-public work on coordination strategies.

- Artifacts delivered with this report.
 - EMT and phasor-aligned models for MT-HVDC/OWF studies (WSCC 9-bus and mini-WECC-derived PSCAD case) suitable for neutral operating scenarios.
 - An IEEE-16-bus-based MVDC loop model demonstrating power scheduling and distributed

Summary

droop concepts at a high level.

- Olympic Peninsula MVDC vs. AC corridor comparison figures and summary tables (rights-of-way and steady-state transfer metrics).
- Curated references and background material for MMCs, MT-HVDC, MVDC, and SSTs to support follow-on research.

Evidence of impact and follow-on work (publications/IP):

- Wind inertial-frequency support (IFR) with real-time management of available kinetic energy to avoid aerodynamic stalling and excessive recovery: invention disclosure on file; external follow-on funding awarded by DOE's WETO; journal manuscript submitted and under review.
- MVDC role assignment and dual-measurement droop for meshed networks: concept validated in simulation; journal manuscript in preparation.
- SST-based autonomous, communication-free coordination across multiple feeders (grid-forming capability on both sides): simulated demonstrations completed; journal manuscript in preparation.
- SST-enabled feeder-level meshed MVDC architectures: concept documentation in preparation for journal submission.
- Olympic Peninsula MVDC closure study: conference paper on steady-state performance and cost/ROW trade-offs in preparation.

Outcomes and next steps (non-proprietary). The project established a reusable modeling stack for EMT-fidelity studies, documented topic-level benefits and trade-offs for MT-HVDC and MVDC, and synthesized SST literature to surface coordination gaps. Novel control methods and architectures developed during the project—e.g., wind-plant IFR with stall-risk management; flexible role assignment/dual-measurement droop in MVDC meshes; and communication-free multi-SST coordination—are intentionally **not** disclosed here; manuscripts are in preparation or under review, and invention disclosures are on file with technology transfer.

Summary

Acknowledgments

This research was supported by the **Energy System Co-Design with Multiple Objectives and Power Electronics (ECOMP) Initiative**, under the Laboratory Directed Research and Development (LDRD) Program at Pacific Northwest National Laboratory (PNNL). PNNL is a multi-program national laboratory operated for the U.S. Department of Energy (DOE) by Battelle Memorial Institute under Contract No. DE-AC05-76RL01830.

Acknowledgments

Contents

Abstr	act			ii			
Sumi	mary			iii			
Ackn	owledg	ments		V			
1.0	Introduction						
	1.1	Why M	IT-HVDC now?	1			
	1.2	Scope	and structure of this report	2			
2.0	Multi	-Terminal	I High Voltage Direct Current (MT-HVDC) Grids	4			
	2.1 Introduction						
	2.2	Modula	ar Multi-Level Converter (MMC)	7			
		2.2.1	Why MMCs became the default for MT-HVDC	7			
		2.2.2	Topology and operating principle	7			
		2.2.3	Submodule options and DC-fault behavior	8			
		2.2.4	Modulation, harmonic performance, and SM energy balancing	9			
		2.2.5	Control architecture (converter level)	9			
		2.2.6	Modeling tiers for EMT and phasor studies	9			
		2.2.7	Parameterization and design trade-offs	10			
		2.2.8	MMCs within MT-HVDC controls (system level touch-points)	10			
		2.2.9	HVDC Station Configurations (VSC-MMC Focus)	10			
	2.3	Use Ca	ase 1 – Preliminary Test Case	12			
		2.3.1	Overview of the WSCC/IEEE 9-Bus System	12			
		2.3.2	Model Implementation and Purpose	13			
		2.3.3	Operational Scenario and Key Observations	14			
	2.4	6, 6					
		2.4.1	Overview	17			
		2.4.2	Mini-WECC EMT Model Development	17			
3.0	Wind Plants as a Power-Electronics–Enabled Source of Inertial Frequency Support						
	• • •						
		Why wind-plant frequency support matters					
	3.2	What system operators need from WPPs					
	3.3	How WPPs provide it					
	3.4	General problems (gaps that motivate further R&D)					
4.0	3.5	-	Focus and Boundaries				
4.0	Medium-Voltage DC (MVDC) and Meshed MT-MVDC Networks						
	4.1	3 , , , , , , , , , , , , , , , , , , ,					
	4.2	Architectures and configurations					
	4.3	Operation and control of MT-MVDC3					
	4.4	Use Case 1 – IEEE 16-bus MVDC Loop3					

Contents

	4.5	4.6 Use Case 2 – Olympic Peninsula (Washington State) MVDC tie-line options	34		
5.0	Solid	-State Transformers (SSTs) as Grid Building Blocks	38		
	5.1	Background and role in a PE-enabled grid	38		
	5.2	Architectures and topologies	38		
	5.3	Primary control and device-level functions	39		
	5.4	5.4 Coordination frameworks in the literature: what exists vs. what is missing	39		
	5.5	Representative use cases for SST-based distribution	40		
	5.6	Scope boundary and IP note for this section	40		
6.0	Conclusions and Outlook				
	6.1	Evidence of impact and follow-on work (publications/IP)	41		
	6.2	Key technical lessons	42		
7.0	Refe	rences	43		

Contents

Figures

Figure 2.1. WSCC 9-bus preliminary use case.	13
Figure 2.2. Switched model test illustrates the phase-to-neutral converter voltage under level-shifted PWM, with a zoom-in panel showing the stepped multi-level staircase consistent with correct carrier disposition and gating sequence	15
Figure 2.3. System-level operation test shows DC-link voltage regulation within the ±0.05 pu band during both symmetric and asymmetric wind ramps, along with nearly equalized AC injections at the onshore MMCs resulting from the droop characteristic—notwithstanding the different corridor lengths	15
Figure 2.4. DC Line 1 trip at t = 5 s: WP1 power is re-routed through Line 3; onshore MMC terminals (DC-voltage droop control) regulate the DC voltage and recover the operating point.	16
Figure 2.5. Illustrative single line diagram of the mini-WECC wind energy integration using an MT-HVDC grid. Areas are scaled to the network size	19
Figure 2.6. Wind farm location and interconnection points (Douville et al., 2024). (a) Location of the wind farm and onshore interconnection points represented by red circles; (b) Wind farm layout with the location of the offshore candidate interconnection points (yellow circles) of the five WPPs	20
Figure 2.7. Frequency response comparison for a 2.251 GW generator trip at Palo Verde: PSS®E phasor vs. PSCAD® EMT. Both traces show consistent electromechanical trends.	22
Figure 3.1. Illustrative drawing of a typical inertial frequency response showing the support phase and the recovery phase of the response. The dashed line shows the undesired case with over-aggressive energy extraction, a deeper speed drop that leads to aerodynamic stalling	26
Figure 3.2. Use Case 1—system frequency response to a generator trip: No IFR, IFR, and IFR—smooth recovery (aggregated wind-plant IFR). Controller parameters and loading are withheld; labels denote generic behaviors only.	27
Figure 3.3. Use Case 1—effect of Aggressive IFR during a generator trip. The Aggressive IFR case depletes kinetic energy and enters a stall trajectory, whereas No IFR avoids this risk but provides no frequency support. Aggressive IFR frequency and power traces are truncated at ~43 s due to model limitations—protection co-simulation is out of scope	27
Figure 3.4. 240-bus mini-WECC EMT—system frequency following a 2.251 GW Palo Verde trip at t = 40 s, with and without wind-plant IFR (aggregate offshore wind ≈10 GW). IFR delays the nadir by ~5.1 s; absolute magnitudes are scenario-dependent.	
Figure 4.1. Use Case 1—IEEE 16-bus MVDC loop. Three MVDC couplers form a controllable ring that supports inter-area transfers and remote feeder coordination via a distributed control layer.	32
Figure 4.2. Baseline (no MVDC): a 20 MW step cannot be supplied without violating substation limits—(a) step at Feeder 1; (b) step at Feeder 2. Each substation is rated 20 MVA	33

Figures viii

around the MVDC ring to supply a 20 MW step at the DC network keeping individual substation flows within the 20 MVA rating	k, while
Figure 4.4. Proposed three-terminal MVDC network is shown by the yellow arro Three DC/AC MMC stations will be located at Amanda Park, Forl Neah Bay	ks, and
Figure 4.5. Cost comparison: 69 kV AC vs ±12 kV DC line (total installed cost vs distance). Crossover distance indicates where MVDC becomes cost-competitive given corridor savings	
Figure 4.6. Cost comparison: 69 kV AC vs ±20 kV DC line (total installed cost vs distance)	
Figure 4.7. Cost comparison: 115 kV AC vs ±12 kV DC line (total installed cost v distance)	
Figure 4.8. Cost comparison: 115 kV AC vs ±20 kV DC line (total installed cost v distance)	
Tables	
Table 2.1. Common MT-HVDC Network Topologies (radial/parallel, series/tap-connected, and meshed/ring) and typical control/prote-implications (VSC-MMC focus)	ction 7
Table 2.2. VSC–MMC HVDC terminal DC-scheme options (concise summary). MR = metallic return; ER = earth/sea return. Sources: (Sharifabac 2016; Van Hertem et al., 2016)	li et al.,
Table 2.3. Coordinates of WPPs and points of interconnection (POI), and straigl distances.	
Table 2.4. Distance Between WPP Stations from North (1) to South (5)	21

Tables

1.0 Introduction

Electric power systems are undergoing a structural transition from centrally dispatched, synchronous-machine–dominated networks to **power-electronics–enabled (PEL) grids** that embed controllable conversion at multiple layers of the infrastructure. Broad deployment of inverter-interfaced generation and storage—wind, solar PV, and battery energy storage (BES)—has shifted system dynamics and created new needs for fast, accurate control of voltage, frequency, and power flows. In parallel, **high-voltage direct current (HVDC)** and **multi-terminal HVDC (MT-HVDC)** have matured into practical tools for long-distance bulk transfer, asynchronous interties, and offshore wind collection, with **modular multilevel converters (MMCs)** becoming the default VSC technology at transmission scale (Sharifabadi et al., 2016; Van Hertem et al., 2016).

1.1 Why MT-HVDC now?

Compared with HVAC, HVDC/MT-HVDC offers controllable active power, independent reactive support at the AC terminals, lower transfer losses over long distances and cables, and freedom from commutation limits, all of which are attractive for interregional ties and offshore corridors (Chou et al., 2012; Kalair et al., 2016; Van Hertem et al., 2016). Multi-terminal topologies further enable power sharing and routing among several converter stations (meshed, ringed, or radial forms), reduce curtailment risk, and allow staged expansion. Their operation typically relies on DC-side coordination methods such as single-slack control, voltage—power droop among multiple terminals, voltage margin schemes, and distributed/secondary supervisory layers (Sharifabadi et al., 2016; Liao et al., 2023; Van Hertem et al., 2016). On the AC side, terminal controls govern voltage, reactive power, and synchronization (grid-forming or grid-following), which must be co-designed with DC droop assignments to avoid adverse interactions (Sharifabadi et al., 2016; Liao et al., 2023).

This report focuses on voltage-source converter (VSC) based MMCs, not LCC schemes. MMCs provide modular scalability, excellent harmonic performance at low switching frequency, and well-understood internal control layers (arm current and energy balancing, circulating-current suppression), which underpin today's MT-HVDC realizations (Sharifabadi et al., 2016). Their capabilities—fast, decoupled P/Q control, ride-through support, and compatibility with weak grids—are central to offshore wind integration and future DC grids (Van Hertem et al., 2016; Sharifabadi et al., 2016).

Because offshore wind plants (OWPs) and other inverter-based resources (IBRs) interface through power electronic controls, their interactions with the bulk system differ from those of synchronous machines. Field experience and studies show that weak-grid conditions can produce low-frequency oscillations (e.g., ~3–4 Hz observed in ERCOT contexts) and that IBR/plant-level controls can excite higher-frequency phenomena up to the kHz range (Fan, 2018a; Fan, 2018b; Zong et al., 2021). Consequently, electromagnetic transient (EMT) studies are required—complementing economic and steady-state planning—to capture fast control interactions, protection behaviors, and AC/DC coupling effects with sufficient fidelity (Ali et al., 2021; NERC, 2025).

To ground the discussion, reduced mini-WECC models are employed as public baselines for EMT analysis and comparative studies. The lineage includes early 179- and 225-bus reduced systems, a widely used 240-bus model for markets/planning (Price & Goodin, 2011), and

Introduction 1

updates that incorporate modern IBR mixes in PSS®E (Yuan, 2020), with EMT implementations reported using vendor translation tools and custom dynamic modules (Wang et al., 2022; Kenyon et al., 2021). Practical phasor-to-EMT transfer relies on tools such as E-Tran and PRSIM to map network and source equivalents and to stage initialization sequences for converters and DC links (Electranix, n.d.; PSCAD, 2023; Cui et al., 2019). Recent work demonstrates EMT mini-WECC cases with integrated offshore wind plants suitable for dynamic benchmarking (She et al., 2024). In parallel, West Coast offshore wind planning highlights transmission constraints and the grid-value proposition of coordinated HVAC/HVDC/MT-HVDC buildouts (PNNL, 2025; DOE, 2025; Douville et al., 2024; NOWRDC, 2023).

1.2 Scope and structure of this report

The report is organized around **power-electronics—enabled grid building blocks** and representative use cases:

- Section 2—MT-HVDC foundations and use case. An overview of MT-HVDC drivers, control concepts (single-slack, droop sharing, supervisory coordination), and MMC modeling is followed by an EMT mini-WECC use case that integrates multiple offshore wind plants. Emphasis is placed on broadly known converter and cable modeling practices and on AC/DC control interactions relevant to system performance. Proprietary controller variants and unpublished configurations are intentionally omitted to protect pending publications and intellectual property evaluations (Sharifabadi et al., 2016; Van Hertem et al., 2016; Liao et al., 2023).
- Section 3—Wind plant frequency support. The role of wind plants in inertial/primary frequency response is summarized with references to established methods (e.g., de-loading strategies and variable droop) and to reliability guidance on fast frequency response (NERC, 2012; NERC, 2020; Aho et al., 2012; de Almeida & Lopes, 2007; Vidyanandan & Senroy, 2013; GE Energy Consulting, 2017). Selected simulations illustrate generic behaviors (energy release and recovery phases) without disclosing novel control approaches under separate review.
- Section 4—Medium-voltage DC (MVDC) networks. Background on MVDC links and meshed MVDC architectures, operating roles (slack versus droop terminals), and basic scheduling/coordination is paired with two use cases: an IEEE 16-bus MVDC loop and an Olympic Peninsula application that explores siting/right-of-way and AC-versus-DC corridor tradeoffs. The section concentrates on steady-state and scheduling impacts; proprietary distributed control choices and role-assignment strategies are not disclosed (Yu et al., 2022; Jambrich et al., 2021; Siemens Energy, 2024).
- Section 5—Solid-state transformers (SSTs). A concise review of SST architectures, demonstration status, and control roles at the distribution edge motivates multi-SST coordination as a grid-architecture problem, distinct from single-device control. Communication-free, feeder-level coordination concepts are discussed at a high level without revealing unpublished methods or parameterizations (Allende et al., 2020; Huber & Kolar, 2019; Cervero et al., 2023).
- Section 6—Conclusions and outlook. Key findings are summarized and near-term research tracks are outlined, including co-design of AC/DC control responsibilities across converters, scalable DC-grid coordination, and distribution-level PEL fabrics.

Introduction 2

Important note on scope boundary: Because this is a public report, details of unpublished or patentable ideas are intentionally withheld. Discussions focus on widely known principles, modeling practice, and generic demonstrations sufficient to motivate the value of PEL building blocks and to frame the questions our research addresses; specific algorithms, controller structures, and parameterizations that are the subject of separate papers or IP review are not disclosed here.

Introduction 3

2.0 Multi-Terminal High Voltage Direct Current (MT-HVDC) Grids

This section develops the multi-terminal HVDC (MT-HVDC) building block within a power-electronics-enabled grid. We outline why MT-HVDC is attracting attention for bulk transfers and offshore wind collection; summarize control concepts (e.g., DC voltage referencing with a designated slack versus distributed DC-droop; power/voltage coordination across terminals); and highlight AC-side interactions at converter points of common coupling. Because converter choice governs system behavior, our focus is voltage-source-converter (VSC) technology using modular multilevel converters (MMCs) rather than line-commutated converters. We describe the MMC operating principles and control layers at a level sufficient for EMT studies, then document the models used here: averaged and switched MMC representations, submarine/export cable models, and two EMT testbeds—a compact WSCC/IEEE 9-bus case for rapid proof-of-concept studies and a public-facing mini-WECC EMT case assembled from a PSS®E base and transferred to PSCAD® via E-Tran. For the larger case, we include a phasor → EMT frequency-response check (largest-unit trip) to confirm consistency over the electromechanical band. The aim is to provide credible, reusable MT-HVDC test environments that capture the dynamics relevant to converter controls, AC/DC interactions, and protection-adjacent behavior without relying on confidential details.

Scope boundary and IP note: This section presents neutral, topic-oriented MT-HVDC material: baseline models (MMC converters, cables, and network data), generic controller structures (e.g., standard AC current control and DC-voltage/droop roles), and representative normal/contingency studies. Content is provided at a level sufficient for use as a study platform for the topics in Sections 3–5, while deliberately omitting any novel control schemes, architectures, parameterizations, or coordination strategies developed in this project. Those innovations remain under journal submission and institutional IP review and will be reported separately.

Section 2.1 frames MT-HVDC motivation and control options; Section 2.2 summarizes MMC operation and control elements used in our models; Section 2.3 presents the 9-bus use case; Section 2.4 documents the mini-WECC EMT case and validation; and subsequent subsections cover cable modeling and representative operating/contingency tests that exercise the MT-HVDC controls in a public, reproducible way.

2.1 Introduction

A multi-terminal HVDC (MT-HVDC) system is a DC transmission network with more than two converter stations; the simplest expansions add a "tap" to an existing point-to-point link, while larger networks may be radial, ringed, or meshed grids (Sharifabadi et al., 2016; Van Hertem et al., 2016). Robust interest in MT-HVDC is driven by the need to (i) integrate large offshore wind power plants (OWPPs), (ii) interconnect asynchronous AC areas, and (iii) increase transfer capability and flexibility while relieving AC congestion (Sharifabadi et al., 2016; Van Hertem et al., 2016).

Modern MT-HVDC grids are enabled primarily by voltage-source converter (VSC) technology implemented with modular multilevel converters (MMCs). MMCs offer high efficiency, fine voltage resolution (low harmonics), scalability, and built-in redundancy, which together make them the preferred VSC platform for today's HVDC and emerging DC grids (Sharifabadi et al., 2016). MMC adoption has been rapid since its introduction in the early 2000s and now

underpins many delivered HVDC projects (Sharifabadi et al., 2016). A few multi-terminal VSC-MMC projects—e.g., Nan'ao (three-terminal) and Zhoushan (five-terminal)—demonstrate real-world feasibility and typical ratings in the ±160–±200 kV class (Sharifabadi et al., 2016).

From a structural standpoint, MT-HVDC systems can be extended from point-to-point links by parallel "taps" (radial development) or by interconnecting nodes to form meshes, improving availability via path redundancy (Sharifabadi et al., 2016; Van Hertem et al., 2016). For offshore applications, planners commonly compare string/radial, ring, and star topologies in collection systems and then connect to the onshore AC grid via VSC-HVDC export systems (Van Hertem et al., 2016). Practical DC busbar arrangements, grounding options, and pole configurations (asymmetrical/symmetrical monopole, bipolar) are also standardized building choices in planned DC substations (Van Hertem et al., 2016).

Compared with AC reinforcements, DC overlays and meshed DC grids promise (i) directional and fast-acting power routing, (ii) decoupled frequency areas, (iii) improved stability margins under disturbances, and (iv) potentially lower losses on long submarine/underground routes (Van Hertem et al., 2016). The "supergrid" vision extends this idea to continental scales, but its realization depends on solutions for DC-side voltage control, load-flow management, and—and critically—DC fault detection and protection (Sharifabadi et al., 2016).

At each terminal, a VSC regulates active (P) and reactive (Q) power into the local AC bus while respecting the converter's PQ capability envelope; steady-state modeling embeds the converter either as a constant-P injection or constant-voltage (UDC) control element if it is tasked with DC-voltage regulation (Van Hertem et al., 2016).

Small MT-HVDC schemes can mimic a two-terminal link by appointing a single "DC-slack" converter to hold the DC voltage, with all other terminals operating in constant-P mode (Van Hertem et al., 2016). However, this centralized approach scales poorly—one terminal must balance the entire network for every disturbance, which can stress that converter and its connected AC area (Sharifabadi et al., 2016). For larger grids, distributed control shares DC-voltage regulation among several converters, often via droop characteristics (power–voltage droop, dead-band droop, voltage-margin control), improving robustness and avoiding single-point dependence (Sharifabadi et al., 2016; Van Hertem et al., 2016). In power-flow studies, this is represented by replacing the single DC-slack with multiple terminals that each contribute according to a droop curve, sometimes combined with constant-P terminals (e.g., OWPP collectors) (Van Hertem et al., 2016).

Unlike AC grids—where power flows depend on phase angles and reactances—DC grid power flows are determined primarily by node voltages and branch resistances. Consequently, DC load-flow management relies on (i) terminal-voltage setpoints/droops and (ii) optional line-inserted DC voltage devices (if/when such power-flow controllers become commercial) (Sharifabadi et al., 2016). For planning and operation, hybrid AC/DC optimal power flow frameworks embed VSC models and DC-grid constraints to co-optimize AC and DC flows (Van Hertem et al., 2016).

DC faults rise very rapidly (millisecond time scale) due to low network impedance and the lack of natural current zero crossings; if not detected and isolated quickly, a pole-to-pole or pole-to-ground fault can collapse DC voltage across the grid and jeopardize connected AC systems (Sharifabadi et al., 2016). Protection must meet stringent requirements for selectivity, speed, reliability, and robustness, with minimal dependence on telecommunication latency (Sharifabadi et al., 2016). Strategies under active development include (a) fast DC circuit breakers (solid-state or hybrid), (b) fault-blocking converter topologies (e.g., full-bridge submodules), and (c) last-resort AC breaker tripping; each involves trade-offs in losses, cost, and service continuity (Sharifabadi et al., 2016). Protection algorithms range from overcurrent/voltage thresholds to traveling-wave and frequency-domain methods; many are validated in EMT simulations or testbeds but remain an active R&D frontier for large MT-HVDC deployments (Sharifabadi et al., 2016).

Europe's offshore programs and North Sea initiatives illustrate staged development—point-to-point OWPP exports evolving toward interlinked assets and, eventually, meshed DC grids as interoperability and DC-voltage standards consolidate (Sharifabadi et al., 2016). Some developers also consider AC-hub concepts (offshore AC pooling between HVDC links) to reduce reliance on DC breakers while enabling power sharing, especially during early build-out phases (Van Hertem et al., 2016). In parallel, control research continues on optimal droop design to guarantee stability across operating points in OWPP-to-AC multi-terminal networks (Van Hertem et al., 2016).

MT-HVDC systems built with VSC-MMC stations can be arranged in a variety of network topologies. The most common patterns are radial/parallel, series/tap-connected, and meshed/ring forms. Table 2.1 summarizes where each is typically used, how power flow is coordinated (e.g., single DC-slack vs. droop-based multi-slack), and what that implies for protection and grounding. The categories follow standard usage in the HVDC-grids literature.

Scope boundary for this report: This report focuses on MT-HVDC fundamentals that underpin our modeling and use case work: (i) converter technology (MMC overview only here; detailed modeling and control appear in Section 2.2), (ii) cable and line models (for both EMT and phasor studies), (iii) AC/DC co-simulation and EMT→phasor model consistency, and (iv) baseline operational scenarios (normal and contingency) that do not disclose proprietary concepts.

Table 2.1. Common MT-HVDC Network Topologies (radial/parallel, series/tap-connected, and meshed/ring) and typical control/protection implications (VSC-MMC focus).

MTDC forms	Dania idaa	How power	Typical control	Ducc	Cana Laguage
MTDC form Series-conn ected	Converters share the same DC current; terminal voltages vary with local power.	flows One series current through all terminals.	emphasis Not a common future path.	Pros Conceptually simple.	Generally not realistic for expanding VSC schemes. (Sharifabadi et al., 2016)
Parallel (radial/tappi ngs)	New terminals tap the existing link; all share a common DC voltage.	Power set by terminal DC voltages; end terminals balance DC voltage.	DC-bus voltage control & power balancing.	Straightforward evolution from point-to-point; easy to add OWFs/loads.	Radial sections lack path diversity; DC voltage coordination is key. (Sharifabadi et al., 2016)
Meshed	Multiple DC paths between nodes.	Flows depend on node voltages and link resistances; parallel paths provide redundancy.	Often needs centralized or decentralize d DC grid voltage controllers; droop or margin methods.	Higher reliability/availab ility; operational flexibility.	More complex protection & coordination; standardization/int eroperability needed. (Sharifabadi et al., 2016)

2.2 Modular Multi-Level Converter (MMC)

2.2.1 Why MMCs became the default for MT-HVDC

The modular multilevel converter (MMC) is a voltage-source converter built from cascaded submodules (SMs) in each arm of a phase leg. Compared with two-level/NPC VSCs, MMCs scale gracefully to high voltages, achieve very low harmonic distortion at modest switching frequency, and offer built-in redundancy. These traits are why MMCs unlocked practical multi-terminal HVDC (MT-HVDC) development and offshore integration at today's voltage and power levels (Sharifabadi et al., 2016; VanHertem_2016).

2.2.2 Topology and operating principle

Each phase has an upper and lower arm, each a series string of SMs and an arm reactor. Two common SMs are the half-bridge (HB) and full-bridge (FB) cells. HB cells insert either +V $_c$ or 0; FB cells can insert +V $_c$, 0, or -V $_c$. The converter synthesizes the phase EMF as half the difference of the two arm voltages; the dc-link voltage appears as the sum. This "sum—difference" view clarifies internal quantities such as circulating current (the common-mode arm current that does not flow to the AC side) and guides the design of energy-balancing and circulating-current suppression controls (Sharifabadi et al., 2016).

Term definitions:

- **SM**: Submodule (a single HB or FB power stage with capacitor).
- HB/FB: Half-bridge / Full-bridge SM types.
- **Circulating current**: Common-mode current that circulates within a phase leg and DC bus; suppressed via control and arm inductance.
- PSC: Phase-Shifted Carrier PWM.
- **NLC**: *Nearest-Level Control* (a staircase modulation that switches in/out the closest integer number of SMs to approximate the reference).

2.2.3 Submodule options and DC-fault behavior

- **HB MMC (baseline):** Lowest semiconductor count and losses; however, during a DC pole-to-pole or pole-to-ground fault, the anti-parallel diodes form an uncontrolled path from the AC grid into the DC fault once the converter is blocked. Clearing typically requires opening AC breakers; DC current tails may persist for hundreds of milliseconds due to network energy. Consequently, HB-only stations need system-level DC protection (e.g., fast DC breakers, FCLs) to enable meshed operation (Sharifabadi et al., 2016).
- **FB MMC (inherent DC-fault blocking):** By producing negative arm voltage, FB stations can force DC current to zero under DC faults, enabling fast isolation with off-load switches and rapid reconfiguration—at the cost of roughly doubling active devices and higher station losses versus HB (Sharifabadi et al., 2016).
- **Hybrid strings (HB+FB mix):** Mixtures can approach FB fault-handling with fewer FB cells, trading cost and loss against fault performance (Sharifabadi et al., 2016).
- Alternatives (AAC): The alternate-arm converter (AAC) uses FB stacks with "director switches" so each arm conducts for half a cycle. It can block DC faults and may reduce capacitor energy, but introduces non-trivial DC-side harmonics and loses some modularity. It sits between HB-MMC and FB-MMC in device count and losses [VanHertem_2016; Sharifabadi et al., 2016).
- Half-bridge MMCs do not inherently block DC faults; they lose current control when the DC bus collapses and therefore require fast DC protection (e.g., DC circuit breakers) and/or network segmentation.
- Full-bridge MMCs can synthesize zero or opposing DC voltage and thus **block DC fault current**, at the cost of higher conduction losses due to more semiconductor paths. See full-bridge MMC capabilities and operating-range discussion.

Practical implication for MT-HVDC: If station cost and efficiency dominate and DC breakers are available, HB MMCs remain attractive; if breaker availability is uncertain or fast fault ride-through and reconfiguration are paramount, FB/hybrid designs or AAC enter consideration (Sharifabadi et al., 2016; VanHertem 2016).

2.2.4 Modulation, harmonic performance, and SM energy balancing

MMCs typically use either PSC-PWM (each SM string uses a triangular carrier phase-shifted across the N SMs) or NLC (Nearest-Level Control), which selects the integer number of inserted SMs closest to the commanded arm voltage, producing a staircase waveform. PSC is straightforward in EMT tools and keeps switching evenly distributed; NLC reduces switching losses but requires careful timing/sorting to limit low-order harmonics (Sharifabadi et al., 2016).

SM capacitor voltages must remain equal while supplying the AC waveform and exchanging DC power. Balancing options include submodule sorting (simple highest-/lowest-voltage first), predictive sorting, tolerance-band (hysteresis) methods, and individual SM-voltage control overlays. The balancing choice interacts with modulation (PSC vs. NLC), switching frequency, and the number of SMs per arm (Sharifabadi et al., 2016).

2.2.5 Control architecture (converter level)

MMC control is layered:

- Inner current control: Either dq-frame PI control (with a PLL to track grid angle) or stationary-frame PR control. These loops regulate AC-side currents (or voltages in STATCOM mode) and typically include circulating-current suppression terms (second-harmonic compensation) to reduce internal losses and ripple (Sharifabadi et al., 2016).
- Outer controls: Common outer loops include active/reactive power control, AC-voltage control (if operating as a grid-forming/STATCOM terminal), and DC-voltage control (one station sets DC voltage; others run power or DC-droop—see Section 2.1). For weak or unbalanced grids, positive/negative-sequence extraction (e.g., DDSRF/DSOGI) and power-synchronization control (PSC*) can improve robustness (Sharifabadi et al., 2016).

Term definitions:

- **PR controller**: Proportional–Resonant controller in stationary αβ frame (tracks sinusoidal references with zero steady-state error).
- PLL: Phase-Locked Loop for grid angle estimation.
- **DDSRF/DSOGI**: Decoupled double synchronous reference frame / Dual second-order generalized integrator methods for sequence extraction.

2.2.6 Modeling tiers for EMT and phasor studies

Depending on the study objective, four standard models trade fidelity vs. speed:

- 1. **SLS** (*Submodule-Level Switched*): explicit switching of each SM—captures switching transients, detailed losses, and balancing, but computationally heavy.
- 2. **SLA** (Submodule-Level Averaged): averages SM switching; still keeps each SM capacitor state.
- 3. **ALA** (*Arm-Level Averaged*): aggregates each arm into lumped variables (sum capacitor voltage per arm).

4. **LLA** (*Leg-Level Averaged*): most compact MMC representation focusing on internal leg dynamics.

Guidance tables map model choice to study type (e.g., protection vs. transient stability). Vectorized implementations in EMT tools (e.g., PSCAD) let you sweep the number of SMs N without redrawing the circuit (Sharifabadi et al., 2016).

For our MT-HVDC use cases (Section 2.3) we will: (i) use ALA for converter-level EMT scenarios (faults, balancing, and control interactions), and (ii) derive reduced phasor equivalents for broader system studies and matching against the mini-WECC phasor case. References that detail averaged MMC models for EMT include Peralta et al. (401-level MMC) and Saad et al. (dynamic averaged MMC for HVDC studies) [Peralta 2012; Saad 2013].

2.2.7 Parameterization and design trade-offs

- Arm inductance (L_arm): Limits di/dt and circulating current; too large → sluggish current control, higher losses; too small → high RMS currents and ripple. Document chosen L arm and its impact on stability margins (Sharifabadi et al., 2016).
- Capacitor sizing (E_cap): Set by allowed SM voltage ripple under worst-case power and modulation; grows with lower switching frequency and with stronger low-frequency power pulsations (e.g., unbalanced or grid-forming operation). Note the assumed ripple % and reserve margin (Sharifabadi et al., 2016).
- **HB vs. FB mix:** Record the assumed HB/FB ratio (if hybrid), the targeted DC-fault performance, and the protection concept (breaker specs vs. inherent blocking) (Sharifabadi et al., 2016).
- Modulation + balancing: State PSC vs. NLC choice and the specific balancing algorithm (sorting/predictive/tolerance-band) used in the EMT model; these materially affect harmonics and switching losses (Sharifabadi et al., 2016).

2.2.8 MMCs within MT-HVDC controls (system level touch-points)

At the MT-HVDC layer, one or more stations regulate DC-link voltage (single DC "slack") and others run P–Q or DC-droop to share imbalances and enable autonomous power sharing. The MMC's outer DC-voltage loop and inner current loops must be tuned to remain well inside station and cable limits while maintaining small-signal damping across the grid. Protection and reconfiguration approaches (DC breakers vs. inherent blocking) determine how fast power can be restored after DC faults—this is a major architectural decision for meshed grids (VanHertem_2016; Sharifabadi et al., 2016).

2.2.9 HVDC Station Configurations (VSC-MMC Focus)

Scope and technology focus.

Throughout this report we consider voltage-source converter (VSC) HVDC based on modular multilevel converters (MMC) as the enabling technology for MT-HVDC grids and OWPP interconnections. Classic line-commutated converter (LCC) schemes are referenced only for context (e.g., commutation dependence on a strong AC system, reactive power consumption,

and harmonic filtering), but detailed LCC design and controls are out of scope (Sharifabadi et al., 2016).

Asymmetrical (monopolar) configuration.

In its simplest long-distance form, one high-voltage pole carries the DC current, with the return via a metallic return conductor or earth/sea electrodes. Metallic return reduces permitting challenges but increases losses versus earth return because of its higher resistance; transformer designs must tolerate DC stress in this configuration. For overhead lines, the negative pole is typically operated at high voltage to cut corona effects (Sharifabadi et al., 2016). A compact treatment of the same arrangement for VSC stations is given in (Van Hertem et al., 2016).

Symmetrical monopole.

Two fully rated, fully insulated conductors operate at ±Un. No steady-state DC stress appears across converter transformers, and grounding is typically high-impedance so that during normal operation no earth current flows. This is the configuration most widely used to date in VSC-HVDC (Sharifabadi et al., 2016). A well-known characteristic is that a single pole-to-ground fault can raise the healthy pole up to ~2·Un until cleared—an important consideration for insulation coordination and protection (Van Hertem et al., 2016).

Bipole.

Two independent poles (+/-) are installed; each has its own converter per terminal. In normal operation, currents in the two poles are balanced, so no return current flows. If regulations permit earth/metallic return, the scheme can continue at ~50% capacity during a single-pole outage; without return, continued operation depends on having a midpoint interlink or reconfiguration. Bipoles offer higher reliability but at higher CAPEX than a single pole (Sharifabadi et al., 2016); see also the VSC-HVDC bipolar description in (Van Hertem et al., 2016).

Homopole.

Both conductors have the same polarity (often negative for overhead lines to reduce corona and radio interference); the return is through earth. Insulation demands on cables/lines are reduced, but the environmental/permitting constraints of earth return apply (Sharifabadi et al., 2016).

Back-to-back (BtB).

Two converters are tied directly DC-to-DC without a long DC transmission element. BtB is used for asynchronous area interties, fast power-flow control, and as a building block in hybrid AC/DC nodes (Sharifabadi et al., 2016).

Table 2.2 summarizes the DC-scheme options commonly used with VSC–MMC HVDC terminals and the situations in which each is preferred.

Grounding and protection implications.

Grounding strategy (solid, resistive, high-impedance) heavily shapes DC fault current and overvoltage behavior and therefore drives insulation coordination and protection design. Symmetrical configurations with high-impedance grounding limit earth currents but can expose the healthy pole to ~2 p.u. during a single pole-to-ground fault; asymmetrical/solidly grounded schemes limit over voltages but allow higher fault current di/dt, mandating faster clearance (Sharifabadi et al., 2016).

Positioning vs. LCC.

For completeness, LCC HVDC remains proven at ultra-high powers and voltages, but it relies on natural commutation, requires strong AC systems, consumes reactive power, and needs extensive AC filtering; by contrast, VSC-MMC provides independent P/Q control, black-start capability, and is the practical enabler of multi-terminal and meshed DC operation (Sharifabadi et al., 2016).

Table 2.2. VSC–MMC HVDC terminal DC-scheme options (concise summary). Abbrev.: MR = metallic return; ER = earth/sea return. Sources: (Sharifabadi et al., 2016; Van Hertem et al., 2016).

HVDC scheme configuration	Key electrical characteristics	Typical applications & design trade-offs
Monopole (asymmetrical; earth/metallic return)	One DC pole (+Vdc) with earth or dedicated metallic return; lowest cable count; no pole redundancy	Short/medium point-to-point links where CAPEX must be minimized; earth return may face regulatory/corrosion limits
Symmetrical monopole (±Vdc/2)	Two conductors with balanced currents; optional midpoint grounding; limited contingency unless metallic return available	Subsea cable links (e.g., OWF export) to avoid continuous ground currents; moderate redundancy
Bipole (±Vdc with neutral/return)	Two poles; neutral at midpoint; can run in monopolar mode on metallic/earth return if one pole is out; highest availability	Long-distance, high-power interconnections; higher CAPEX and station complexity but superior reliability and maintenance flexibility
Homopole (same-polarity conductors)	Two conductors at same polarity; typically uses earth return; high current/low voltage; corrosion/EMF concerns	Rare today; niche, short-distance high-current applications where ground return is permissible
Back-to-back (co-located terminals)	Converters in one station; no DC line; DC bus only; isolates asynchronous AC systems with tight controllability	Compact interties and power-flow control between asynchronous grids; no transmission corridor required

2.3 Use Case 1 - Preliminary Test Case

2.3.1 Overview of the WSCC/IEEE 9-Bus System

The WSCC (WECC) 3-machine/9-bus system—often referred to as the IEEE 9-bus test system—is a compact, didactic benchmark widely used for transient stability and controls research. It consists of three synchronous generator areas supplying three load buses through a simple meshed 230-kV transmission backbone. Because it retains the essential electromechanical interactions while keeping network size tractable, it is well suited for early proof-of-concept studies and rapid controller iteration (KIOS, 2013).

This "small but expressive" footprint makes the 9-bus system a practical stepping stone toward the multi-inverter, multi-terminal studies developed later in this report, and aligns with the project's stated goal to explore power-electronics—enabled grid building blocks through staged, control-oriented models before scaling up to MT-HVDC/MT-MVDC architectures. A single-line diagram of the use case system is shown in Figure 2.1.

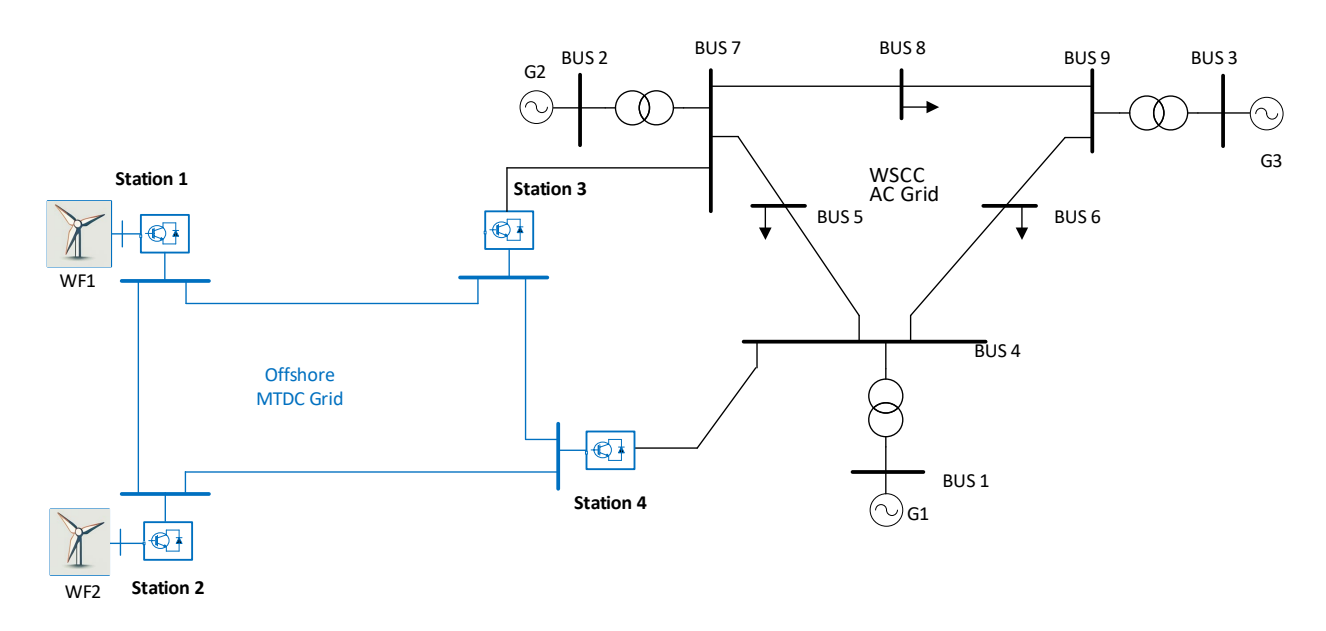


Figure 2.1. WSCC 9-bus preliminary use case.

2.3.2 Model Implementation and Purpose

This use case was built to validate proof-of-concept designs under EMT-fidelity while preserving iteration speed. The model is implemented in MATLAB/Simulink (Simscape Electrical − Specialized Power Systems). Two aggregated offshore wind plants (OWPs) are represented using the DFIG phasor model, then interfaced to the EMT network via a dedicated phasor ↔ EMT interface block (to keep the network solution in EMT while retaining fast plant-level parametric sweeps on the DFIG side). Transmission distances for the four 230-kV corridors (Line1–Line4) are set to 300 km, 300 km, 100 km, and 260 km, respectively, to capture diversity in electrical lengths while remaining within a compact study system (KIOS, 2013).

Two MMC-based VSC terminals are modeled to represent the shore-side converter stations; both averaged-value and switched MMC representations are available. The switched representation is used selectively to validate modulation and arm-level dynamics; the averaged model is used for the broader operational testing to accelerate simulation throughput. Conceptually, control follows standard MMC practice (outer power/DC-voltage loops, inner current control, arm-energy/circulating-current management), and DC-voltage droop is employed across shore-side terminals for autonomous power sharing without a single fixed DC slack (Sharifabadi et al., 2016).

Figure 2.2 illustrates the phase-to-neutral converter voltage under level-shifted PWM, with a zoom-in panel showing the stepped multi-level staircase consistent with correct carrier disposition and gating sequence.

2.3.3 Operational Scenario and Key Observations

To exercise both symmetric and asymmetric operating points without exposing any project-specific control innovations, we apply only wind-speed ramps at the two OWPs and observe HVDC terminal responses and onshore power sharing:

- At t = 10 s and t = 20 s, wind speeds at both OWPs increase in steps of +2 m/s (from 5 to 7 m/s, then to 9 m/s).
- At t = 40 s and t = 60 s, asymmetry is introduced: OWP-1 increases by +2 m/s (then +4 m/s), while OWP-2 decreases by −1 m/s (then −2 m/s).

Across all steps, (i) the DC pole-to-pole voltage at the shore-side converters remains within ±0.05 pu of its reference, and (ii) the onshore injection remains approximately balanced between the two shore terminals despite unequal cable lengths and unequal generation, indicating that DC-voltage droop—without any single designated DC slack—achieves the intended autonomous power sharing and fast DC-side power balancing (Sharifabadi et al., 2016). These behaviors are canonical for droop-coordinated VSC terminals in MTDC studies and are shown here solely to establish a neutral baseline response.

Figure 2.2 shows DC-link voltage regulation within the ±0.05 pu band during both symmetric and asymmetric wind ramps, along with nearly equalized AC injections at the onshore MMCs resulting from the droop characteristic—notwithstanding the different corridor lengths.

Figure 2.3 shows the response of the MT-HVDC when DC line 1 trips at t=5s. It can be seen that the power from WP1 is wheeled through Line 3 and the DC voltage is well regulated by the shore units.

Figure 2.3 illustrates the MT-HVDC system response to a DC Line 1 outage initiated at t = 5 s. Following the trip, active power exported by WP1 is automatically rerouted via Line 3, while the onshore MMC terminals—operated with standard DC-voltage droop—stabilize the DC pole voltage and restore it to the pre-fault setpoint. These cases use conventional droop-based DC-voltage regulation only; no novel control methods are disclosed.

The switched MMC verifies modulation, arm current behavior, and energy balancing at the device/block level (Figure 2.2), while the averaged MMC is preferentially used for the multi-step operational test (Figure 2.3) to keep run-times short. Both representations are standard in MMC practice; switching-level models are used to verify wave-shape and internal energy flows, and averaged models for control and system-level EMT studies (Sharifabadi et al., 2016).

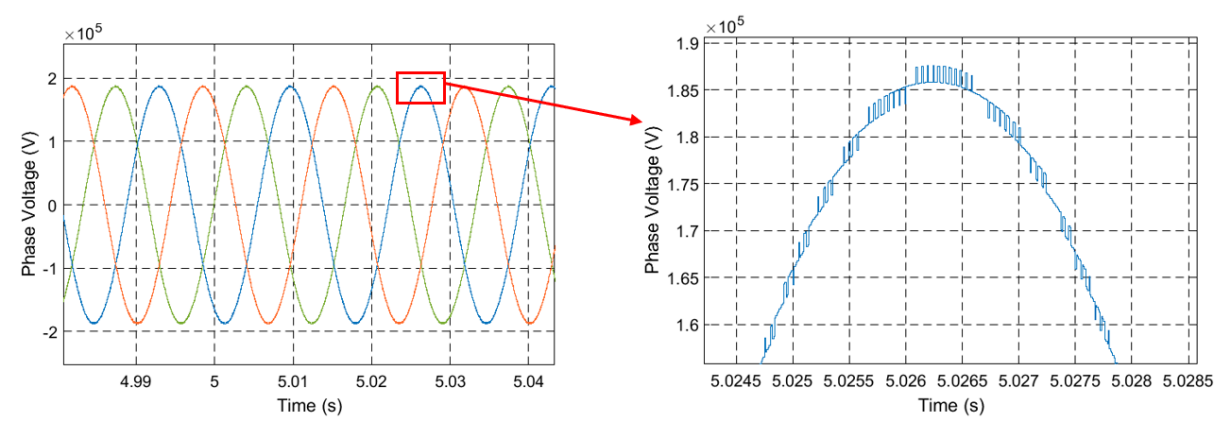


Figure 2.2. Switched model test illustrates the phase-to-neutral converter voltage under level-shifted PWM, with a zoom-in panel showing the stepped multi-level staircase consistent with correct carrier disposition and gating sequence.

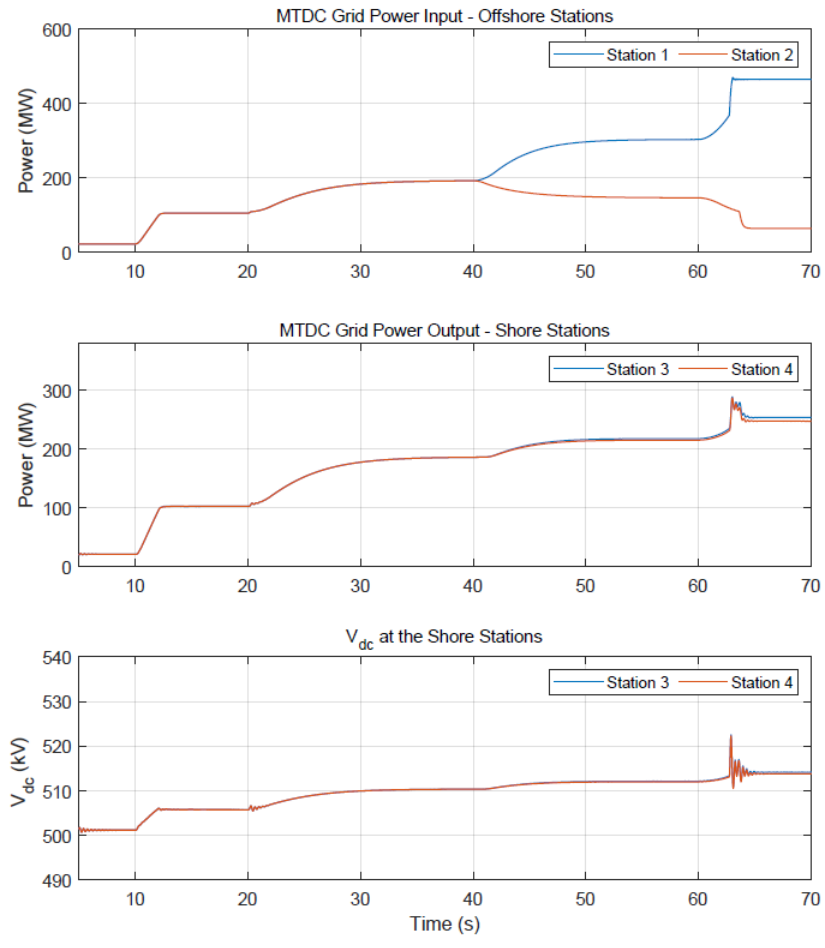


Figure 2.3. System-level operation test shows DC-link voltage regulation within the ±0.05 pu band during both symmetric and asymmetric wind ramps, along with nearly equalized AC injections at the onshore MMCs resulting from the droop characteristic—notwithstanding the different corridor lengths.

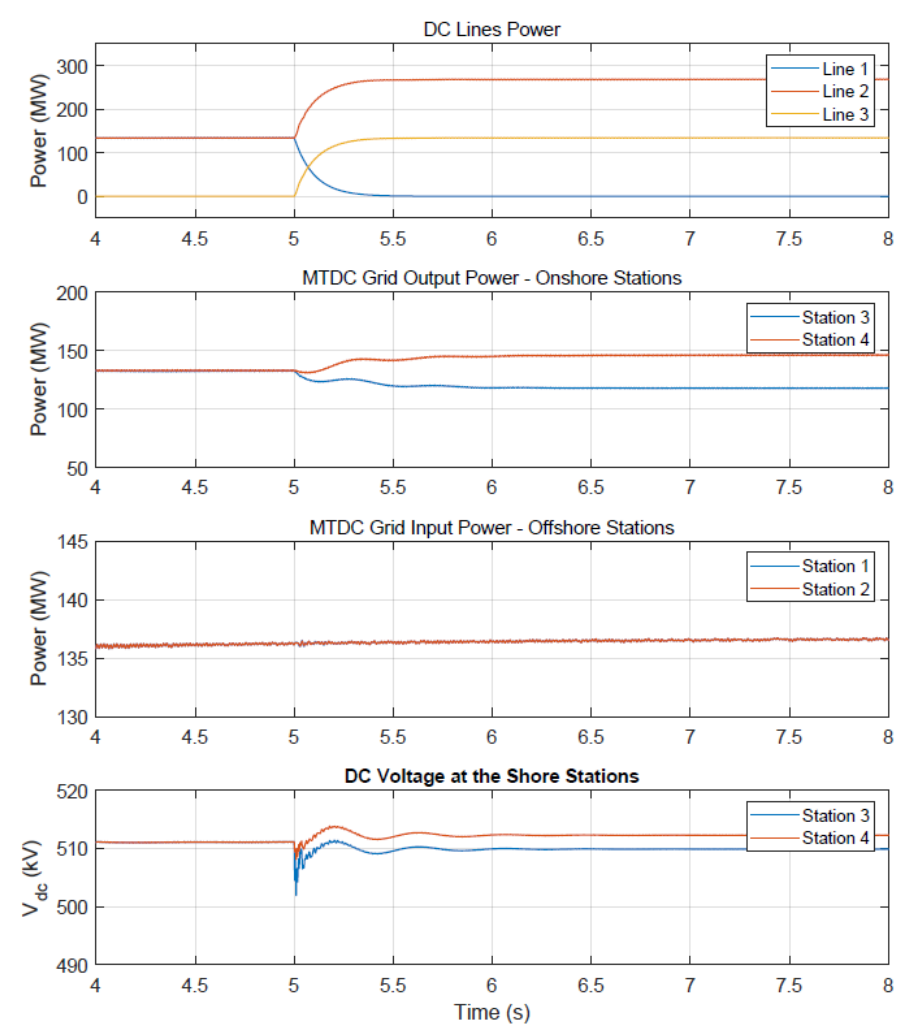


Figure 2.4. DC Line 1 trip at t = 5 s: WP1 power is re-routed through Line 3; onshore MMC terminals (DC-voltage droop control) regulate the DC voltage and recover the operating point.

2.4 Use Case 2 – Offshore Wind Energy Integration Using MT-HVDC

This section assembles a public-facing electromagnetic-transient (EMT) baseline for integrating offshore wind farms (OWFs) into the Western Interconnection using modular multilevel converter (MMC) multi-terminal HVDC (MT-HVDC) interfaces. We summarize the motivation and planning context, outline the Mini-WECC 240-bus foundation case, and describe the workflow from PSS®E phasor to PSCAD® EMT via E-Tran. We then document OWF placements, onshore points of interconnection (POIs), approximate submarine cable corridors, and candidate MT-HVDC terminals (coordinates and distances). Finally, we present a frequency-response consistency check between the phasor and EMT cases for a large generator trip, followed by normal and contingency EMT runs. Novel control concepts developed in this project are intentionally omitted here to preserve publication and IP options; the models and results shown reflect broadly known practice.

2.4.1 Overview

Offshore wind farms (OWFs) are a key decarbonization resource for the Western Electricity Coordinating Council (WECC) system. Recent planning work indicates that West Coast transmission capacity is a primary constraint on integrating OWFs at scale, and that a coordinated interregional build-out leveraging high-voltage alternating current (HVAC), high-voltage direct current (HVDC), and multi-terminal HVDC (MT-HVDC) can materially relieve that constraint and improve overall system benefits (Douville et al., 2024; Chou et al., 2012; Sun_2021; Liao et al., 2023). In short, HVDC/MT-HVDC provides controllable bulk transfers, asynchronous ties between regions, and the option to collect and export offshore wind via multi-terminal architectures—raising net benefits while supporting progress toward carbon-free grids.

Because OWFs and other inverter-based resources (IBRs) are power-electronics interfaced, their interactions with the grid's electromechanical dynamics differ markedly from synchronous machines. Field experience and studies show that weak grid conditions can produce low-frequency oscillations (e.g., 3–4 Hz as observed in ERCOT) and that OWF/IBR controls can excite higher-frequency phenomena into the kHz range (She et al., 2024; Fan, 2018a; Zong et al., 2021]. Economic planning alone is therefore insufficient; electromagnetic transient (EMT) analysis is required to assess fast dynamics, control interactions, and protection behavior with sufficient fidelity [Ali et al., 2021; Lin_2018]. To keep this public report focused on broadly known concepts, proprietary implementation details are intentionally omitted; new methods are reserved for separate publications and IP review.

2.4.2 Mini-WECC EMT Model Development

Background on mini-WECC models. Several "mini-WECC" reduced-order models exist for system studies: early 179-bus and 225-bus versions [Jung_2002; Yu_2009], followed by a 240-bus model for market/planning analysis (Price & Goodin, 2011). A later 240-bus update incorporated increased IBR penetration in PSS®E using WECC 2018 data (*Yuan, 2020*), and a PSCAD® version was subsequently assembled using PRSIM (PSCAD, 2023) components with custom dynamic modules (Wang et al., 2022). As of the time of writing in that reference, public access to the PSCAD case was limited.

Scope of this work. Building on (*Yuan, 2020*), we developed a public-facing EMT case in PSCAD to serve as a baseline for OWF integration and control-interaction studies. The workflow was:

Starting point: 240-bus mini-WECC in PSS®E with IBR dynamics per (Yuan, 2020).

Network transfer: AC network data converted using E-Tran (Electranix) from the phasor domain to PSCAD-compatible EMT representations (Cui et al., 2019).

Module completion: Replacement/augmentation of generic models with self-developed EMT control modules where needed for IBRs and HVDC/MMC terminals.

Initialization: Sequential initialization to ensure DC links, converter internal states, and OWF collector systems converge cleanly prior to disturbance studies.

System characteristics. Per (*Yuan, 2020*), the 240-bus mini-WECC totals ≈291 GW of generation, including ≈59 GW of grid-following (GFL) IBRs (utility-scale PV, onshore wind, distribution PV). That mix provides a credible base for exploring OWF injections and MT-HVDC interfaces. For visualization, Figure 2.4 presents an illustrative single-line diagram of the 240-bus mini-WECC along with the radially connected five wind-power plants (WPPs), where areas/states are scaled to network size. Locations of the offshore plants and onshore interconnection points are shown in Figure 2.5.

Key elements—such as total power rating and plant locations—are slightly modified from (Douville et al., 2024), while keeping the combined rating of the five WPPs at approximately 10 GW. Candidate coordinates for offshore/onshore MMC stations are adapted from (Douville et al., 2024). Approximate straight-line distances to onshore points are summarized in Table 2.3, and approximate distances among the offshore MMC stations are summarized in Table 2.4.

Given the phenomena cited above—low-frequency oscillations in weak areas, converter-control interactions, and high-frequency effects—an EMT model is the appropriate tool to examine (i) ride-through and fault-recovery behavior of OWFs, (ii) AC/DC control interactions around MT-HVDC terminals, and (iii) the sensitivity of system damping to controller settings and short-circuit ratios (She et al., 2024; Fan, 2018a; Zong et al., 2021; Ali et al., 2021).

To confirm consistency over the electromechanical band, we compared frequency responses between the PSS®E phasor case and the PSCAD EMT case for a large-disturbance event: tripping the largest generator at Palo Verde, Arizona (≈2.251 GW, ~1.5% of total online generation). Figure 2.6 shows that the PSCAD frequency trajectory closely tracks the PSS®E result in terms of nadir and primary oscillation content, supporting use of the EMT case as a baseline for fast-dynamics and control-interaction studies.

To keep this public report focused on broadly known concepts, we intentionally refrain from describing novel control methods or proprietary configurations. The case illustrates established modeling practice (e.g., MMC-HVDC terminals, standard OWF collector systems, and representative IBR controls) and supports the generic studies reported later (normal and contingency operation). Any new concepts developed in this project are reserved for separate publications and intellectual-property evaluation.

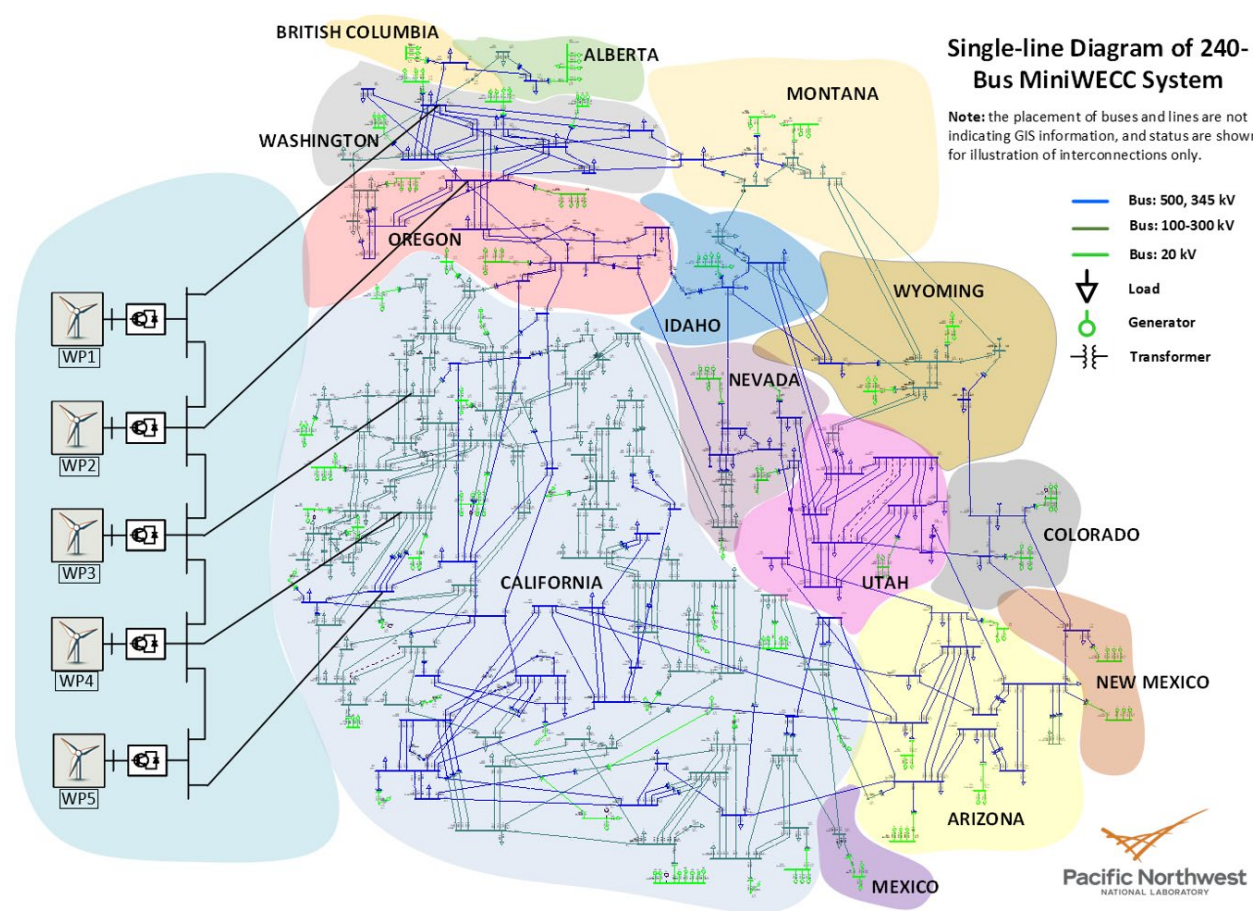


Figure 2.5. Illustrative single line diagram of the mini-WECC wind energy integration using an MT-HVDC grid. Areas are scaled to the network size.

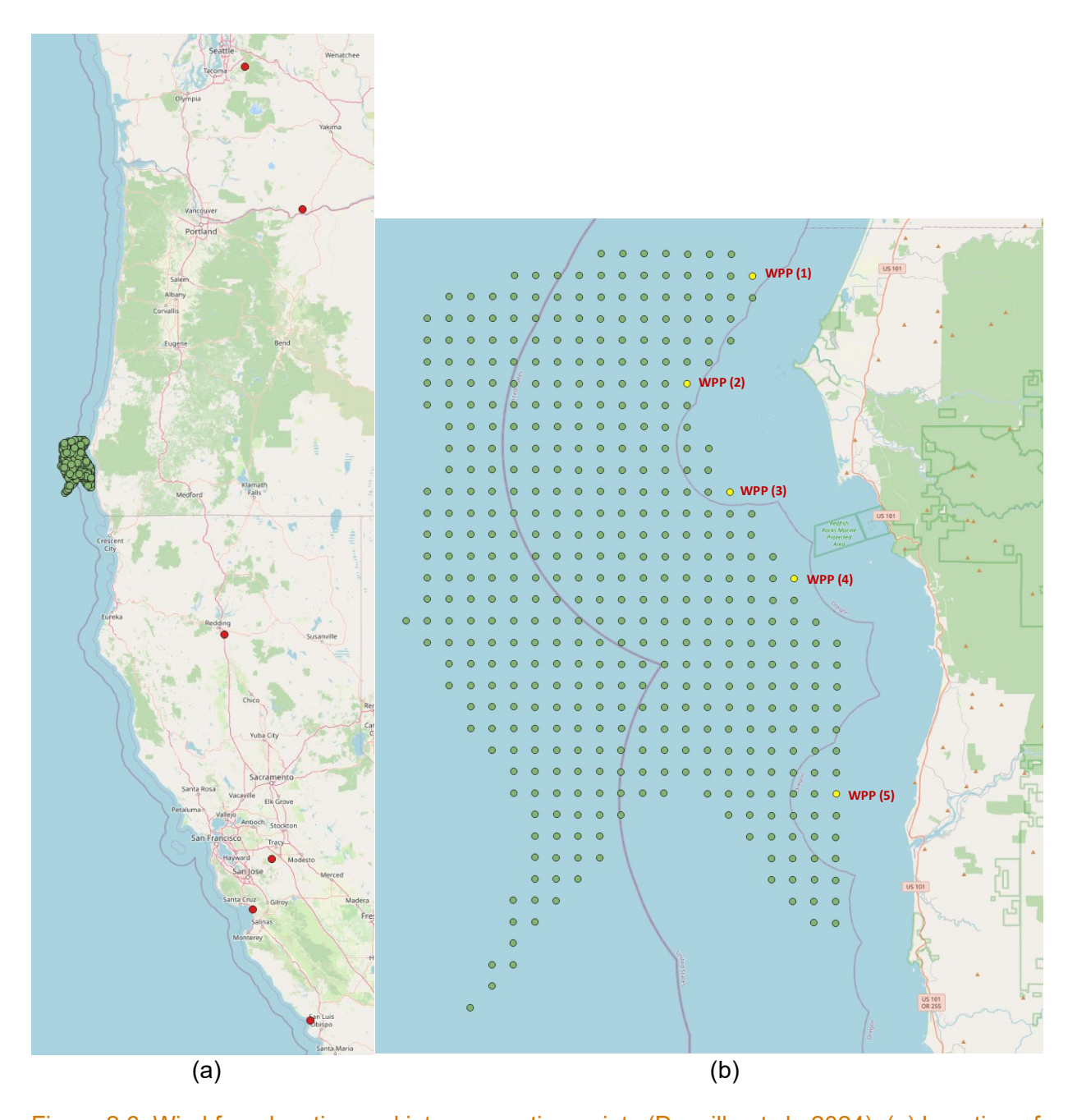


Figure 2.6. Wind farm location and interconnection points (Douville et al., 2024). (a) Location of the wind farm and onshore interconnection points represented by red circles; (b) Wind farm layout with the location of the offshore candidate interconnection points (yellow circles) of the five WPPs.

Table 2.3. Coordinates of WPPs and points of interconnection (POI), and straight-line distances.

WPP Coordii		ordinates	inates POI Coordinates			
POI Name	Latitude	Longitude	Latitude	Longitude	Distance (km)	Distance (mile)
WCASCADE, WA	42.7805	-124.6851	47.3471	-122.124	545.060 km	338.685 mi
JOHN DAY, OR	42.8362	-124.6604	45.67762	-120.738	444.423 km	276.151 mi
COTTONWOOD, CA	42.7053	-124.6092	40.3987	-122.265	324.193 km	201.444 mi
TESLA, CA	42.6301	-124.558	37.71241	-121.565	603.598 km	375.059 mi
MOSSLAND, CA	42.4659	-124.5102	36.90315	-121.807	660.732 km	410.559 mi

Table 2.4. Distance Between WPP Stations from North (1) to South (5)

	WPP Coordinates from North t South		_		
POI Name	Latitude	Longitude	To WPP	Distance (km)	Distance (mile)
(1) JOHN DAY, OR	42.7805	-124.6851	to (2)	6.596 km	4.098 mi
(2) WCASCADE, WA	42.8362	-124.6604	to (3)	10.301 km	6.401 mi
(3) COTTONWOOD, CA	42.7053	-124.6092	to (4)	9.352 km	5.811 mi
(4) TESLA, CA	42.6301	-124.558	to (5)	18.895 km	11.741 mi
(5) MOSSLAND, CA	42.4659	-124.5102	to (1)	45.145 km	28.052 mi

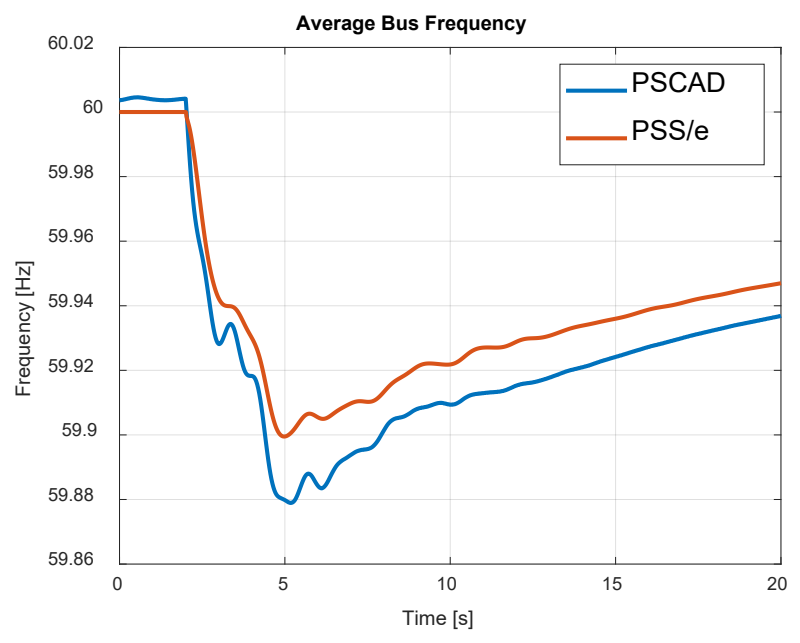


Figure 2.7. Frequency response comparison for a 2.251 GW generator trip at Palo Verde: PSS®E phasor vs. PSCAD® EMT. Both traces show consistent electromechanical trends.

3.0 Wind Plants as a Power-Electronics-Enabled Source of Inertial Frequency Support

As synchronous generation retires and inverter-based resources (IBRs) scale, interconnection inertia declines and frequency can fall faster for a given contingency. In that context, operators are turning to *fast* frequency services and codifying requirements that balance inertia, fast frequency response (FFR), and primary frequency response (PFR) to avoid under-frequency load shedding and preserve reliability (NERC, 2020; NERC, 2012). In this report we focus on the subset of fast services delivered through wind plant power-electronic interfaces—**inertial frequency response (IFR)**—and on complementary active-power controls (e.g., droop with headroom) that provide PFR from wind. Together, these capabilities function as grid *building blocks* that power electronics can deliver where rotating mass is no longer plentiful NERC, 2020.

Modern wind turbine generators (WTGs) can momentarily inject additional active power by extracting rotational energy from their drive-train inertia—an "inertia-based FFR" that the industry increasingly distinguishes from the older, ambiguous term "synthetic inertia" (NERC, 2020). Typical magnitudes are on the order of 5–10% of instantaneous output for several seconds, bounded by mechanical and control limits and followed by an energy-recovery phase whose shape matters for system performance (NERC, 2020; GE Energy Consulting, 2017). This makes IFR valuable in the first seconds after a disturbance, but it also introduces a recovery trade-off that must be managed to avoid secondary dips or adverse turbine dynamics (GE Energy Consulting, 2017).

Sustained **primary** response from wind requires *headroom* (intentional deloading) and a droop-like active-power control that increases output as frequency falls. The literature has shown multiple ways to realize this—from early DFIG-based schemes that combine converter and pitch controls while operating on a deloaded power curve, to later approaches that adapt the droop online to prevailing wind conditions [Almeida_2007; Vidyanandan_2013]. Industry tutorials synthesize these options and their practical limits (measurement and actuation latencies, pitch wear, energy opportunity cost, and coordination at the plant controller) (Aho et al., 2012). In short, IFR helps *arrest* frequency, while deloaded PFR helps *stabilize and restore* it; both are implementable with today's wind plant controls and both are mediated by power-electronic interfaces.

Consistent with the protection of intellectual property and future publications, this section uses conventional control constructs only. We define terms and constraints (arresting energy, recovery behavior, headroom policies), recap established schemes and reliability drivers, and then use two prepared study cases (Use Case 1 and the mini-WECC EMT case from Section 2) to **illustrate** generic IFR/PFR behaviors under representative generator-trip events. Any novel control elements developed during this project are **not** described here and are reserved for separate publications.

3.1 Why wind-plant frequency support matters

Modern frequency control is being stressed by (i) larger credible contingencies relative to on-line inertia, (ii) higher instantaneous penetration of inverter-based resources (IBRs), and (iii) the need for faster, accurately shaped response to keep the system away from UFLS thresholds.

Industry guidance now treats fast frequency response (FFR) as an essential reliability service, complementary to primary frequency response (PFR) and slower secondary/tertiary actions (NERC, 2020; NERC, 2012). In simple terms: inertia, plus prompt active-power injection and well-behaved recovery, are all needed to meet nadir and ROCOF objectives in low-inertia conditions.

Wind-power plants (WPPs) can contribute along two well-established paths:

- **Kinetic-energy-based response** (often called "synthetic inertia," "IBFFR"): brief power boost via controlled rotor-speed reduction.
- **Deloading-based PFR/FFR**: maintain headroom (curtailment) and use droop or other active-power controls to inject additional power during events.

Both are technically feasible at the turbine and plant levels, with control and coordination strategies surveyed in academic/industry literature [(ho et al., 2012; de Almeida & Lopes, 2007; Vidyanandan & Senroy, 2013].

3.2 What system operators need from WPPs

Operator needs are framed by three knobs: **contingency size**, **on-line inertia**, and **speed/magnitude of active-power response**. When inertia is low, the system must receive energy sooner (sub-second to a few seconds) to arrest the frequency decline; and that fast action must hand off smoothly to sustained PFR so frequency neither rebounds nor dips again during recovery (NERC, 2020; GE Energy Consulting, 2017). Practically, this means: rapid detection/triggering, shaped power injection, and carefully designed **recovery** that avoids withdrawing energy too soon.

3.3 How WPPs provide it

Deloading for droop-based response. A large body of work shows DFIG-based and full-converter machines can participate in primary regulation when pre-curtailed (headroom) and controlled with fixed or variable droop (de Almeida & Lopes, 2007; Vidyanandan & Senroy, 2013). Variable droop improves smoothing and can enhance nadir relative to fixed droop, at the cost of energy curtailment and with practical limits tied to rotor-speed, pitch, and converter current capabilities (Vidyanandan & Senroy, 2013).

Kinetic-energy (IBFFR). Turbines can momentarily exceed available aerodynamic power by extracting rotor kinetic energy; the benefit is a very fast boost. The challenge is ensuring the **post-event recovery** is not detrimental (e.g., inducing a second dip) and that the **rotor-speed excursion** stays within safe aerodynamic/mechanical bounds (NERC, 2020; GE Energy Consulting, 2017).

Plant-level coordination. Active-power controls exist at both turbine and plant levels (AGC set-points, plant controllers that allocate effort across turbines). Coordinated strategies determine how much each turbine contributes and how recovery is paced so the aggregate response is smooth and grid-friendly (Aho et al., 2012).

3.4 General problems (gaps that motivate further R&D)

1. **Energy availability vs. deliverability**. WPP response is constrained by two energy "buckets": (i) headroom (deloading) and (ii) rotor kinetic energy. The limiting factors are

converter current, torque/thermal limits, pitch/speed bounds, and OWF collector/export interface limits. Practically, a response that looks acceptable at the plant POI can still push individual turbines near aerodynamic or mechanical limits if not managed holistically (Aho et al., 2012).

- Recovery-phase side effects. A fast boost must hand off to sustained response without causing a second frequency dip. Both NERC guidance and the GE advisory work emphasize that "brief injection followed by withdrawal" is problematic if recovery timing and magnitude aren't engineered alongside the initial boost (NERC, 2020; GE Energy Consulting, 2017).
- 3. Aerodynamic stability at low winds. Under low wind speeds, aggressive responses can drive rotor speed too low, risking loss of aerodynamic torque margin and unstable operation if not bounded. The literature on variable droop explicitly notes the need to guard lower droop/response limits to avoid very low rotor speed leading to instability (Vidyanandan & Senroy, 2013). This is fundamentally an energy-budgeting and constraint-management problem.
- 4. Triggering and false positives. Very fast action requires dependable event detection. GE's system studies show tradeoffs among frequency-threshold versus ROCOF triggers and highlight false-trigger risks and PMU/WAMS opportunities—issues that directly affect how early and how hard WPPs should respond (GE Energy Consulting, 2017).
- 5. **Service economics and energy opportunity cost**. Deloading-based PFR/FFR carries opportunity costs (lost energy). NERC and GE both argue for market/rule frameworks that value response shape, speed, and sustainability—i.e., pay for reliability-relevant attributes, not just nameplate MW (NERC, 2020; GE Energy Consulting, 2017).

Enabling well-behaved frequency support from WPPs is one of the power-electronics—enabled grid building blocks we are documenting—i.e., a grid-support capability unlocked by converter controls and plant coordination, not by new rotating inertia.

3.5 Study Focus and Boundaries

This project centers on event-phase energy release and post-event recovery from WPPs—framed as a real-time management of available kinetic energy and headroom so that the aggregate response improves nadir and ROCOF without pushing turbines into aerodynamic stall regimes or causing excessive recovery-phase draw from the grid:

- **Event phase:** Define practical envelopes for active-power boost that respect rotor-speed, torque, and converter limits while still being fast enough to materially improve nadir in low-inertia conditions.
- Recovery phase: Shape the return of rotor speed and plant output so the system does not
 experience a second frequency dip, and individual turbines avoid low-speed operating
 pockets associated with aerodynamic instability; again, we remain method-agnostic here
 and omit implementation specifics.

Figure 3.1 shows an Illustrative drawing of a typical inertial frequency response showing the support phase and the recovery phase of the response. The dashed line shows the undesired case with over-aggressive energy extraction, a deeper speed drop that leads to aerodynamic stalling.

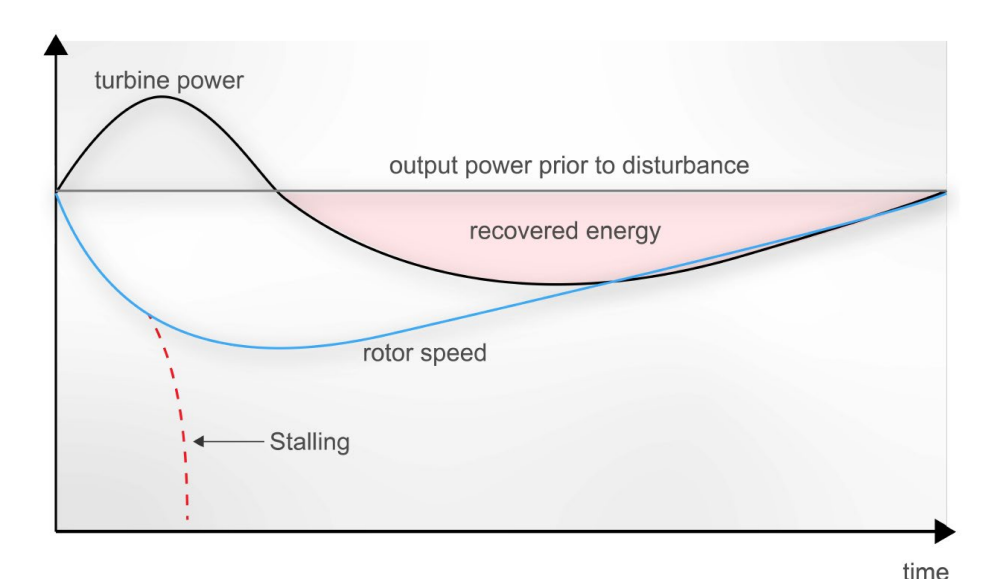


Figure 3.1. Illustrative drawing of a typical inertial frequency response showing the support phase and the recovery phase of the response. The dashed line shows the undesired case with over-aggressive energy extraction, a deeper speed drop that leads to aerodynamic stalling.

contrasts the system frequency with no wind FFR, a baseline wind-FFR implementation, and a variant with a smoothed recovery ramp intended to reduce secondary dips and improve settling. Only frequency is shown to keep the focus on system-level outcomes; controller specifics are outside the scope of this public report.

To ground the discussion, Figure 3.2 shows the system frequency from Use Case 1 (WSCC 9-bus EMT model) following a generator trip. Three traces are compared: No IFR, IFR, and IFR—smooth recovery. The plot illustrates how conventional inertial frequency response (IFR) reduces ROCOF and improves the nadir relative to No IFR, while shaping the recovery ("smooth recovery") limits the post-event frequency which results in further improvement in the response.

Figure 3.3 uses the same Use Case 1 disturbance to highlight a pitfall: overly aggressive IFR that overdraws kinetic headroom. With otherwise nominal conditions, aggressive settings improve the initial nadir first but drive the rotor through the aerodynamic stall region during the recovery phase which leads to instability and tripping the wind plant. The No IFR trace is included as a baseline. Under the aggressive setting, the simplified EMT testbed (which omits detailed protection and certain saturation limits) enters a non-physical regime shortly after the onset of aerodynamic stall; accordingly, the Aggressive IFR frequency and power traces are truncated at \sim t = 43 s to avoid misinterpretation.

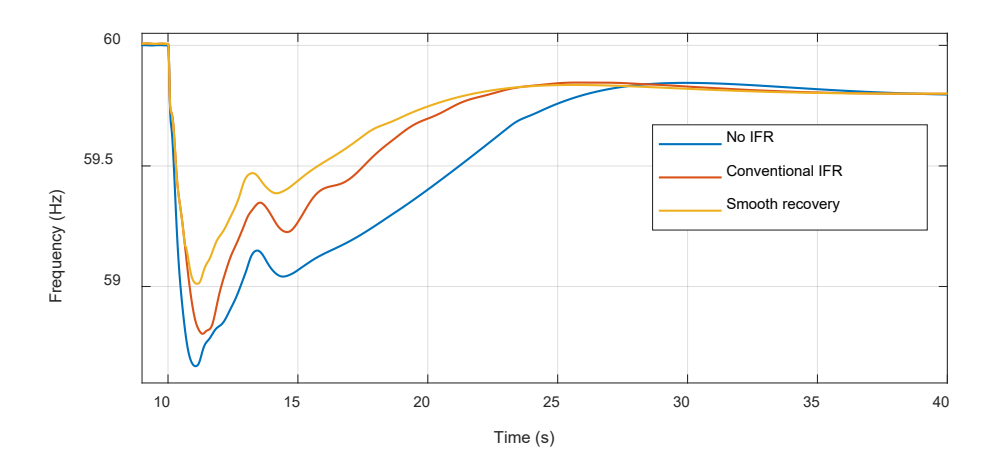


Figure 3.2. Use Case 1—system frequency response to a generator trip: No IFR, IFR, and IFR—smooth recovery (aggregated wind-plant IFR). Controller parameters and loading are withheld; labels denote generic behaviors only.

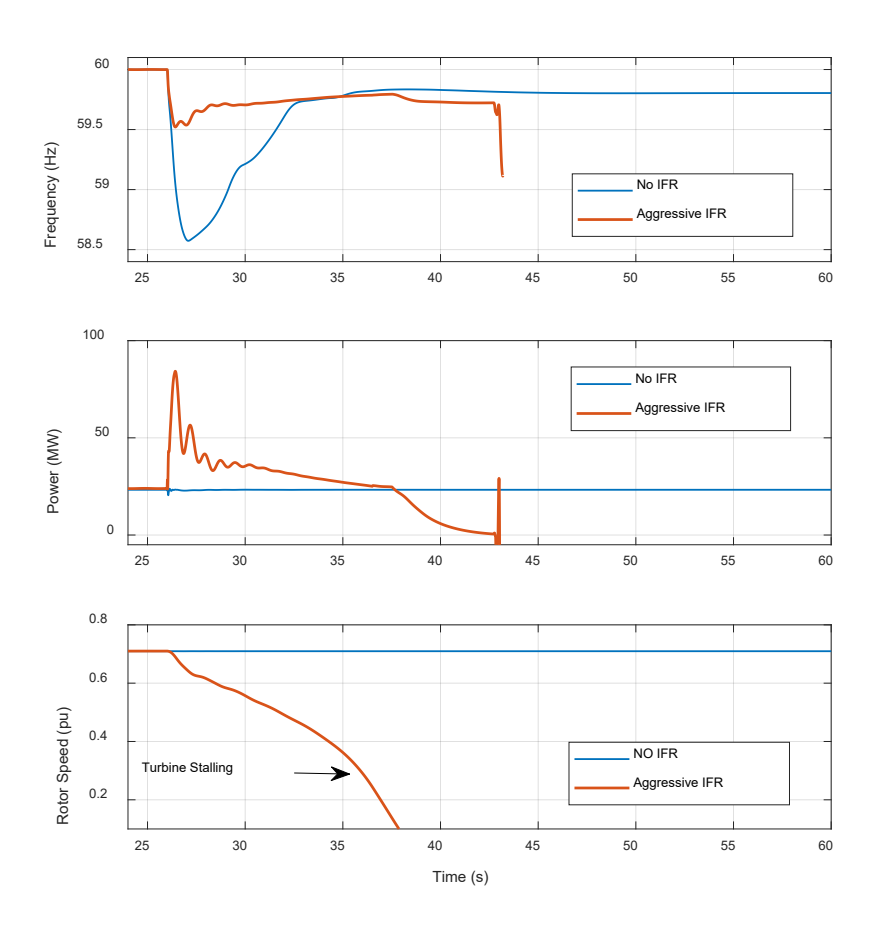


Figure 3.3. Use Case 1—effect of Aggressive IFR during a generator trip. The Aggressive IFR case depletes kinetic energy and enters a stall trajectory, whereas No IFR avoids this risk but provides no frequency support. Aggressive IFR frequency and power traces are truncated at ~43 s due to model limitations—protection co-simulation is out of scope.

To gauge the system-level impact, Figure 3.4 reports the 240-bus mini-WECC EMT case from Section 2. The largest Palo Verde unit (\approx 2.251 GW) is tripped at t = 40 s. Even with an aggregate offshore wind nameplate of \approx 10 GW (small relative to overall system capacity), enabling IFR delays the nadir by \sim 5.1 s, materially easing primary-reserve pickup and under-frequency protection margins. Absolute frequency values depend on reserve posture and tuning; only the timing shift is emphasized here.

To protect pending intellectual property, implementation details and controller design choices underlying the 'smooth recovery' behavior are intentionally withheld; an invention disclosure has been filed and a DOE-WETO award is supporting the follow-on R&D.

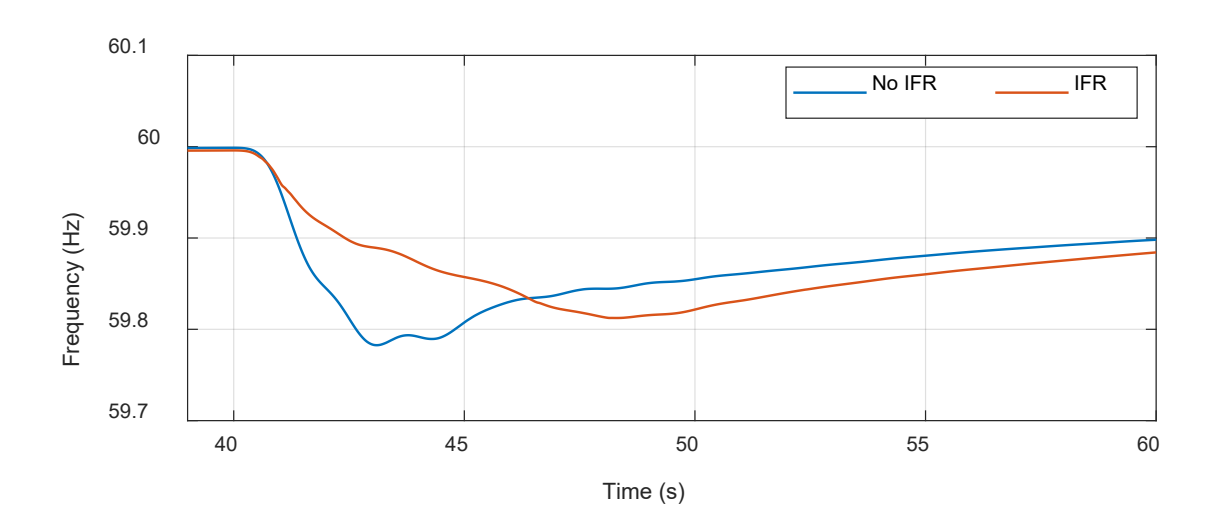


Figure 3.4. 240-bus mini-WECC EMT—system frequency following a 2.251 GW Palo Verde trip at t = 40 s, with and without wind-plant IFR (aggregate offshore wind $\approx 10 \text{ GW}$). IFR delays the nadir by $\sim 5.1 \text{ s}$; absolute magnitudes are scenario-dependent.

4.0 Medium-Voltage DC (MVDC) and Meshed MT-MVDC Networks

This section reviews medium-voltage direct current (MVDC) links and multi-terminal MVDC (MT-MVDC) networks as power-electronics—enabled building blocks for sub-transmission and distribution grids. We summarize motivations, practical architectures, and operation/control patterns for point-to-point (PtP), ring, and meshed topologies; highlight the option to convert existing AC corridors to DC; and then present two use cases (IEEE 16-bus and the Olympic Peninsula). Throughout, converters are VSC-based MMCs (voltage-sourced converter, modular multilevel converter). The research focus in this project is on greater control flexibility—including role assignment (e.g., DC-slack vs. power-controlled terminals), droop allocation, and autonomous role re-assignment in meshed MT-MVDC—but implementation details are intentionally withheld here for IP and publication reasons (Yu et al., 2022; Jambrich et al., 2021; Siemens Energy, 2024).

4.1 Background, drivers, and benefits

MVDC brings controlled power flow, higher corridor capacity per conductor material, reduced reactive effects (no steady reactive power transfer), and the ability to couple asynchronous or weak areas—capabilities that align with high-DER, electrification-driven grids. CIGRE's JWG C6/B4.37 frames MVDC as a practical extension of HVDC concepts into distribution and sub-transmission, enabling "horizontal" ties between distribution areas, improved utilization of existing assets, and flexible network operation; it also catalogs ring/meshed configurations appropriate for public grids (Yu et al., 2022). These attributes mirror, at smaller scale, the well-established benefits of HVDC and enable point-to-point links, DC "couplers," and meshed multi-terminal MVDC (MT-MVDC) grids (Yu et al., 2022).

On the siting/corridor side, MVDC at medium voltage allows lower structure heights and narrower rights-of-way (ROW) (e.g., simple wood-pole or compact steel construction below treetops), which can materially reduce visual impact and land cost—key drivers in built or sensitive environments (Siemens Energy, 2024).

From an efficiency/economics perspective, break-even distances for underground cable links at MV levels are short: ≈ <10 km at 10 kV rising to ≈ 30 km at 33 kV, after which MVDC losses + station penalties compare favorably to MVAC. That makes MVDC viable for many sub-transmission and distribution interties, especially where corridor constraints dominate (Yu et al., 2022).

Several utilities are evaluating AC-to-DC conversion to unlock higher transfer on existing lines without new RoW. Technical brochures and project reports (e.g., ANGLE-DC, conversion of 33 kV AC circuits in the UK) document feasibility, configurations, and measured transfer-capacity increases after conversion (Yu et al., 2022).

From the vendor perspective, MVDC conversions can increase transmitted power by ~20–80% on existing corridors while improving grid stability (e.g., STATCOM functionality from VSC terminals) (Siemens Energy, 2024).

4.2 Architectures and configurations

Network topologies. Practical MVDC configurations include PtP, radial, ring, and meshed networks; rings/meshes are natural for area interties and for closing loops around geographic features (e.g., peninsulas) to improve reliability and controllability (Yu et al., 2022).

Converter poles. Symmetrical monopole (±Vdc) and bipole are prevalent, with hybrid variations depending on grounding and redundancy needs; symbols and building blocks follow the TB conventions. (Yu et al., 2022).

Station technology. Implementations are typically VSC-MMC at MV levels; commercial product lines (e.g., MVDC PLUS®) are standardized by type ratings, with grid services such as bidirectional active power control and AC-side voltage support (Siemens Energy, 2024; Jambrich et al., 2021).

AC to DC line conversion. Demonstrations like ANGLE-DC (conversion of existing 33 kV AC feeders to MVDC) report ~23% capacity increase without building new corridors—illustrating a cost-effective upgrade path when station costs are balanced by ROW constraints (Yu et al., 2022).

4.3 Operation and control of MT-MVDC

MVDC operation is anchored by voltage-source converters (VSCs)—often modular multilevel converters (MMCs)—providing four-quadrant control at each terminal. In multi-terminal operation, one or more terminals regulate DC voltage (the "DC slack"), while others regulate power or current setpoints. In practice, operators may employ:

Single-slack: one terminal regulates DC voltage; others run in power control.

Distributed slack via DC droop: several terminals share DC-voltage regulation using droop characteristics, which improves sharing and resilience to terminal trips.

Hierarchical dispatch: a master station (local or remote) issues active/reactive setpoints and ramp rates; terminals enforce setpoints subject to local limits (Yu et al., 2022).

On the AC side, terminals can operate in grid-forming (AC-voltage/angle) or grid-following (P/Q or V/VAR) modes to support feeder voltages and reactive power management as needed— with no single universal rule; role assignment is system-dependent and can be scheduled to meet operating objectives (Yu et al., 2022).

Interfacing layers (e.g., MVDC↔HVDC or MVDC↔LVDC) often use DC–DC converters (isolated or non-isolated; bi-directional or unidirectional), with topology choices driven by power-flow direction and galvanic-isolation needs (Yu et al., 2022).

Converter-level loops (inner current/synchronization and outer P/Q or V control) and system-level controls (assignment of DC-slack terminals and droop-sharing across multiple terminals) are the standard toolset for MT-MVDC operation. There is no universal rule for how many terminals serve as DC-voltage "slacks" versus power-controlled units; operators tune this by objective (congestion relief, loss minimization, voltage margins) and by network strength on each side (Yu et al., 2022).

The section's novel contribution concerns flexibility in role assignment and new forms of droop behaviors to enable grid-forming or grid-supporting operation on either side as operating conditions change. In this report only the motivation and study setups are described; control logic and design details are reserved for subsequent publications and IP evaluation.

4.4 Use Case 1 – IEEE 16-bus MVDC Loop

A compact IEEE 16-bus-derived AC network was augmented with three MVDC couplers arranged to form a controllable ring/mesh across selected corridors. The case is used to exercise power scheduling (inter-area transfers), DC-slack assignment (single-slack vs. distributed droop), and re-assignment under contingencies. The use case network is shown in Figure 4.1. The developed control strategy can operate autonomously to respond to DERs generation and Load demand. For remote power flow coordination of feeders, distributed control is used.

Without the MVDC loop in service, no single feeder can supply an additional 20 MW step at Feeder 1 or Feeder 2 without exceeding the 20 MVA substation ratings, as illustrated in Figure 4.2a–b. With the MVDC loop enabled, the distributed controller utilizes available headroom across substations to supply the same 20 MW step while keeping individual substation flows within the 20 MVA rating. The MVDC couplers route power around the ring so that neither feeder's local substation is overloaded, as shown in Figure 4.3, where a 20 MW load is connected to the MVDC network.

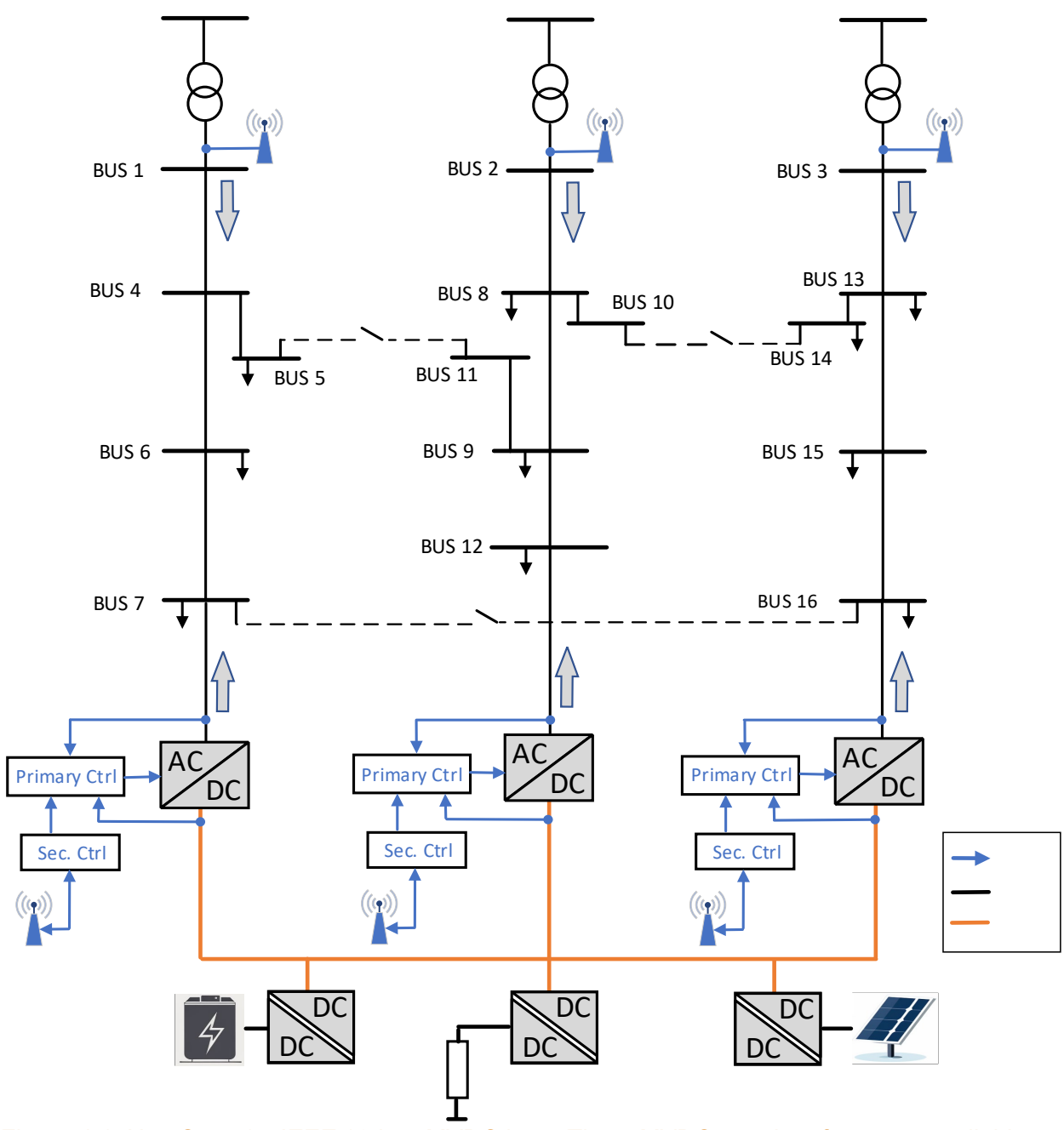


Figure 4.1. Use Case 1—IEEE 16-bus MVDC loop. Three MVDC couplers form a controllable ring that supports inter-area transfers and remote feeder coordination via a distributed control layer.

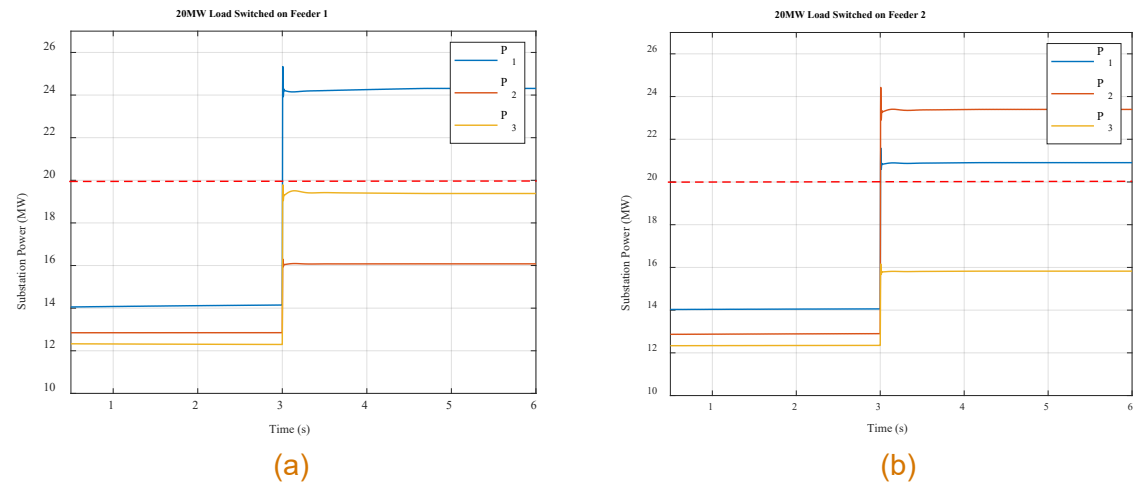


Figure 4.2. Baseline (no MVDC): a 20 MW step cannot be supplied without violating substation limits—(a) step at Feeder 1; (b) step at Feeder 2. Each substation is rated 20 MVA.

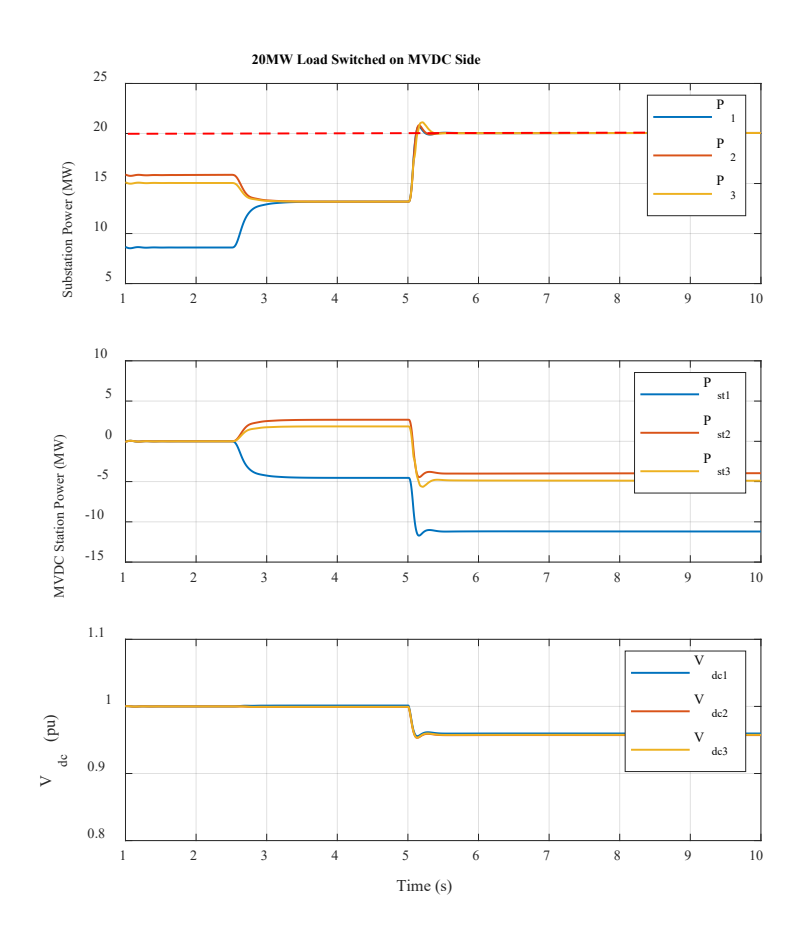


Figure 4.3. MVDC-enabled sharing: the distributed controller uses substation headroom around the MVDC ring to supply a 20 MW step at the DC network, while keeping individual substation flows within the 20 MVA rating.

4.5 4.6 Use Case 2 – Olympic Peninsula (Washington State) MVDC tie-line options

The northwest Olympic Peninsula (Forks → Neah Bay) is long and radial, with sparse load pockets, forested terrain, and limited ROW—making reliability back-feed and future growth challenging. The study compares AC tie options versus MVDC links to close the loop and enable controllable transfers. This work proposes two tie lines. One from Neah Bay to Forks and a second from Forks to Amanda Park as shown in Figure 4.4. The first tie line (Neah Bay to Forks) would create a ring configuration under which most outages could be isolated while minimizing the number of customers affected. The second tie line (Forks to Amanda Park) adds a second source to the OP system. With this configuration if the feed from Sappho is lost, the system could be supplied from Amanda Parks via Forks. The combination of (i) narrower corridors & lower structures at MV levels and (ii) controlled power exchange across asynchronous/weak areas favors MVDC, especially where land and permitting dominate total cost (Siemens Energy, 2024; Yu et al., 2022).



Figure 4.4. Proposed three-terminal MVDC network is shown by the yellow arrows. Three DC/AC MMC stations will be located at Amanda Park, Forks, and Neah Bay.

For a representative 69 kV AC option, the study estimates total cost \approx \$736 k/mile (\approx \$472 k/mile excluding land), with additional storage costs (\sim \$976 k) included in the scenarios where storage was assumed necessary.

For a 115 kV AC option, the study estimates $\approx \$798$ k/mile ($\approx \$509$ k/mile excluding land). Cost analysis shows that, as line length grows, ± 12 kV and ± 20 kV MVDC tie lines become more cost-effective than AC alternatives—driven largely by land/ROW costs and the ability to use smaller, lower-cost line structures. For a ~ 100 -mile combined buildout, the study projects >\$35 M savings (± 12 kV MVDC vs. 69 kV AC) and >\$40 M savings (± 12 kV MVDC vs. 115 kV AC), with similar favorable results for ± 20 kV cases. Figures 4.5–4.8 plot total installed cost versus route length for AC and MVDC alternatives at two MV bases and two DC pole voltages; the crossover distances reflect ROW/structure savings for DC offset against converter station costs.

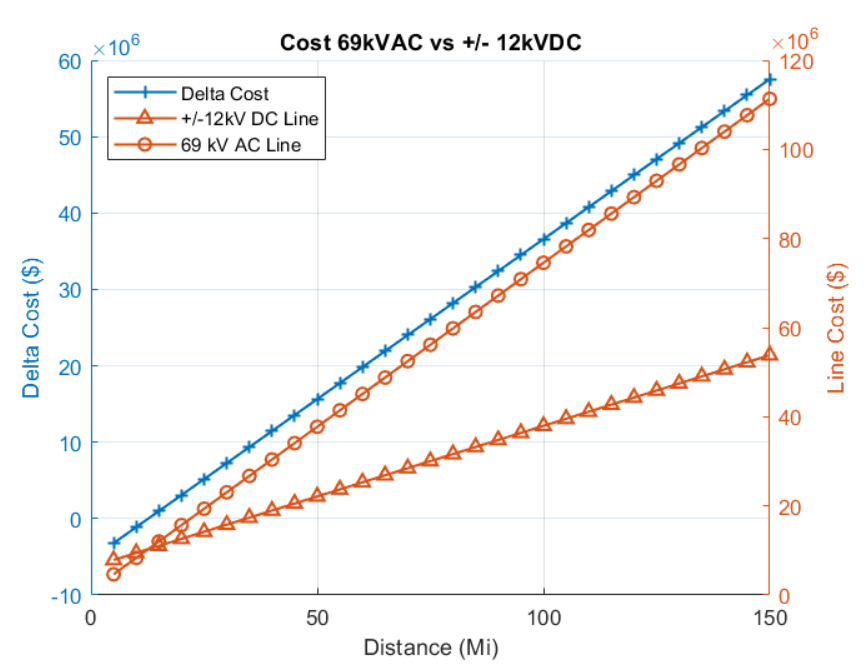


Figure 4.5. Cost comparison: 69 kV AC vs ±12 kV DC line (total installed cost vs distance). Crossover distance indicates where MVDC becomes cost-competitive given corridor savings.

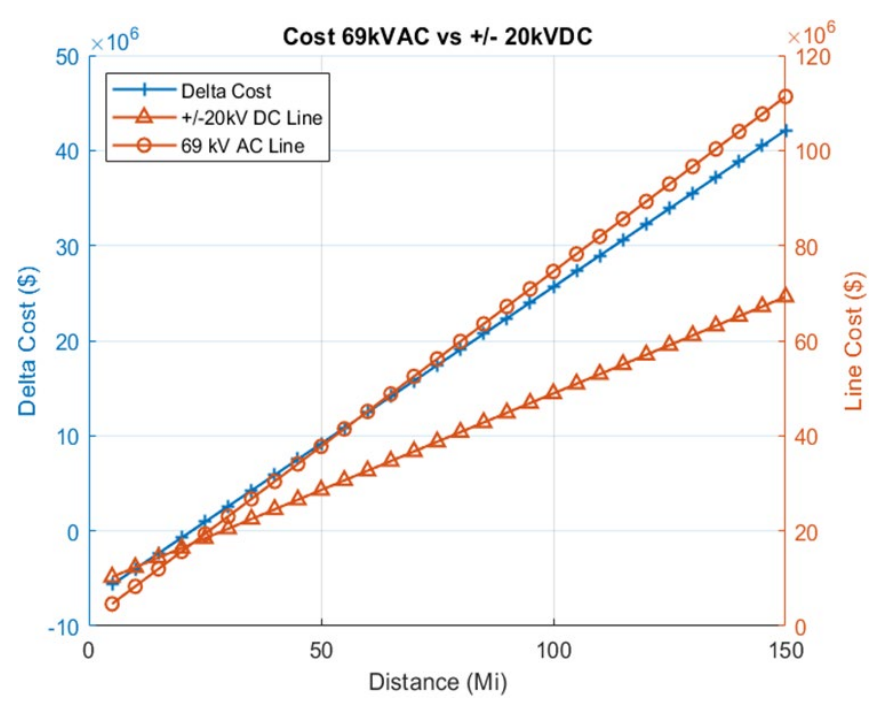


Figure 4.6. Cost comparison: 69 kV AC vs ±20 kV DC line (total installed cost vs distance).

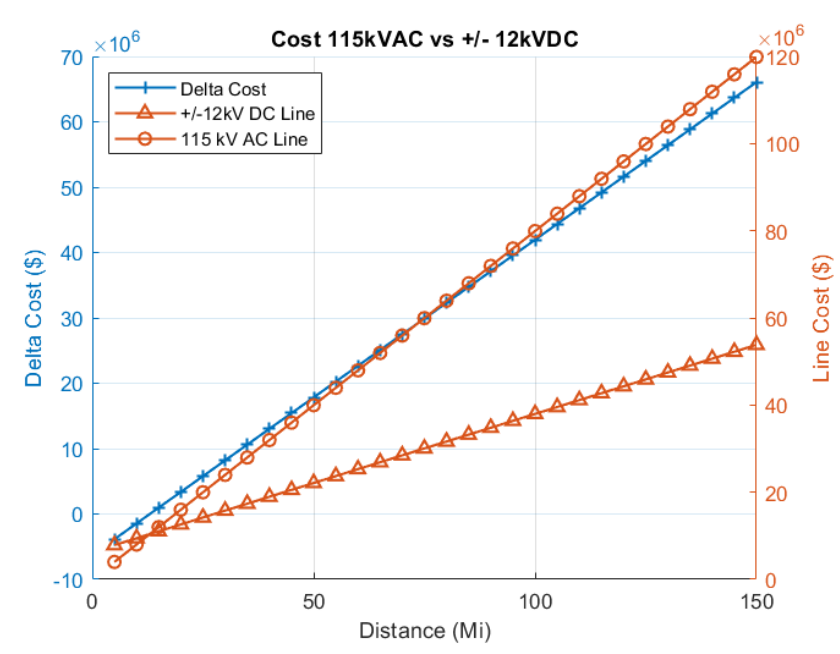


Figure 4.7. Cost comparison: 115 kV AC vs ±12 kV DC line (total installed cost vs distance).

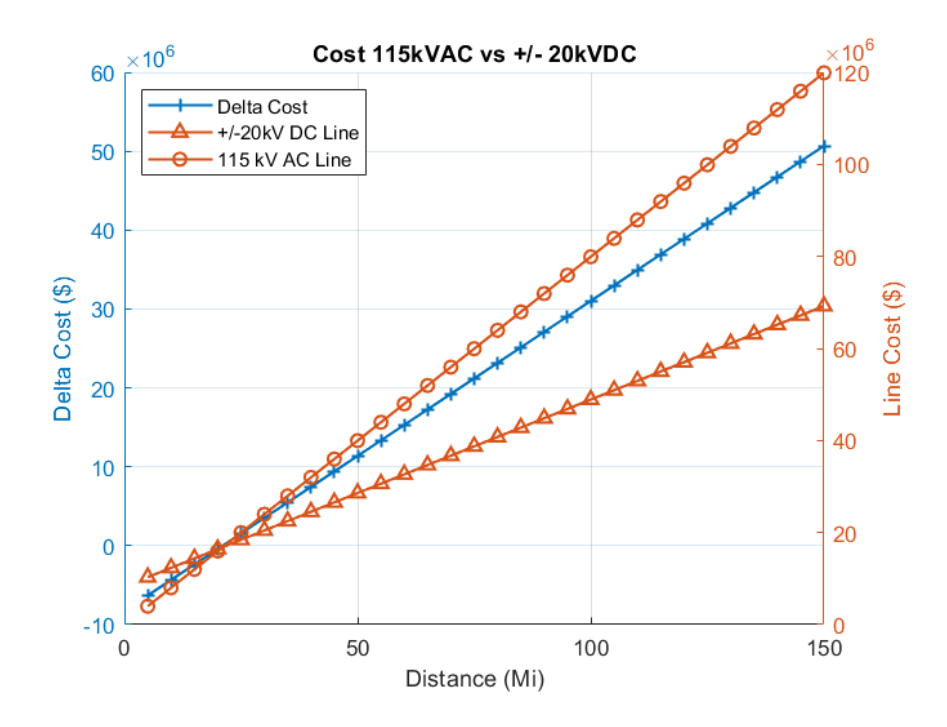


Figure 4.8. Cost comparison: 115 kV AC vs ±20 kV DC line (total installed cost vs distance).

5.0 Solid-State Transformers (SSTs) as Grid Building Blocks

5.1 Background and role in a PE-enabled grid

Solid-state transformers (SSTs)—also called *smart transformers (STs)*—combine high-frequency (HF) isolated power conversion with software-defined control to perform voltage transformation and advanced grid functions at the medium-/low-voltage (MV/LV) interface. Compared with magnetic transformers, SSTs provide bidirectional power flow, fast dynamic control, and native interfacing of AC and DC subsystems through their internal DC link(s), positioning them as architectural elements in a *power-electronics (PE)*—*enabled grid* rather than merely device-level replacements (Allende et al., 2020; Huber & Kolar, 2019; Saleh et al., 2019a; Saleh et al., 2019b). Across feeders, they can improve voltage quality, support frequency and volt/var control, host hybrid AC/DC operation, and coordinate distributed energy resources (DERs) such as PV, battery energy storage (BES), and EV charging (Allende et al., 2020; Huber & Kolar, 2019).

From a system perspective, SSTs are nodes that can sense and regulate *both sides* of the interface (MV and LV) while arbitrating energy across an internal DC link. This enables feeder-level services (power flow steering, contingency support, fast restoration) that conventional transformers cannot deliver and aligns with DOE's TRAC roadmap viewing solid-state power substations as a pathway to resilient, flexible distribution grids (DOE TRAC, 2020).

5.2 Architectures and topologies

Most practical SSTs use a multi-stage structure that separates functions: an AC/DC front-end, an isolated DC/DC stage with HF transformer, and a DC/AC back-end (or DC bus) to serve local loads and DERs. Representative realizations include:

- **Dual-Active-Bridge (DAB)—based DC/DC** stages, often multiport for DER integration; variants mix phase-shift and resonant modulation to trade efficiency vs. bandwidth (Sun et al., 2020).
- MMC-based HF SSTs, which leverage modular multilevel structures for high conversion ratios and low passive component stress; low-inertia DC SST control has been demonstrated for predictive power regulation (Martin et al., 2022), and HF-MMC DC-DC concepts with three-winding transformers for DC flux cancellation have been explored (Gray et al., 2022).

Recent advances in SiC MOSFETs/diodes, HF magnetics, and power-dense packaging underpin the realizations above by improving efficiency, power density, and voltage capability (Saleh et al., 2019a; Huber & Kolar, 2019). A growing body of demonstrators and pilots indicates rising technical maturity, while large-scale deployment still hinges on cost, standardization, and interoperable control frameworks (Cervero et al., 2023).

5.3 Primary control and device-level functions

On a single SST, primary loops typically include:

- AC-side voltage and frequency regulation (grid-forming mode) or current/Power-factor control (grid-following), with fast volt/var support (Shah & Crow, 2016; Huber & Kolar, 2019).
- **DC-link energy management** to balance MV/LV power and maintain internal voltages; energy- or power-feedforward schemes enhance dynamic balance (Ge et al., 2015).
- **DER port control** for PV, BES, EV—coordinated via droop-like laws, MPC, or hierarchical dispatch (Sun et al., 2022; Qu et al., 2022; Rahman et al., 2020; Yu et al., 2014).
- **Virtual inertia/damping** and frequency-based power control implemented at the converter, including VSM-style behaviors in SST contexts (Wald et al., 2024).

These capabilities are well documented for *single-SST* installations and enable robust local microgrid operation, islanding at one node, and power-quality enhancement (Allende et al., 2020; Huber & Kolar, 2019; Rahman et al., 2020).

5.4 Coordination frameworks in the literature: what exists vs. what is missing

Most published coordination strategies address one SST orchestrating its local AC/DC terminals or adjacent microgrids with either centralized or distributed logic (often communications-assisted) (Rahman et al., 2020; Yu et al., 2014; Ren et al., 2023; Li et al., 2023). A parallel thread connects multiple SST sites via their DC links to form meshed hybrid microgrids, typically with discrete operating modes and rule-based power scheduling; this has been shown for two-SST or small multiport cases and focuses on DC-link meshing rather than feeder-level AC coordination (Hrishikesan & Kumar, 2021; Hrishikesan et al., 2022; Hrishikesan & Kumar, 2020; Das et al., 2021; Das et al., 2022; Das et al., 2020).

Gap #1 – Multi-SST, feeder-level AC coordination. Published works generally do not address *autonomous* coordination across multiple SSTs on the AC side (i.e., across feeders and substations) that can (i) share grid-forming responsibilities, (ii) allocate roles/limits in real time, and (iii) sustain a fully islanded, multi-feeder network without relying on reliable high-bandwidth communications. Existing DC-meshing studies and single-SST schemes are valuable, but they do not close this systems-level gap.

Gap #2 – Role assignment and scheduling under changing conditions. In conventional leader/follower SST operation, the load-side converter regulates AC voltage while the grid-side converter regulates the internal DC link; that division constrains how *several* SSTs can share grid-forming duties when islanded and how they transition roles during contingencies. Scalable methods for *role assignment* (who regulates what, where, and when) are largely absent in the literature (Huber & Kolar, 2019; Allende et al., 2020).

Gap #3 – Plug-and-play, communication-light primary control. There is a need for primary-control laws that ensure safe operation when supervisory communications are degraded or absent, with stable interactions among DERs, BES, and upstream resources across *many* SST nodes (DOE TRAC, 2020).

5.5 Representative use cases for SST-based distribution

SSTs naturally enable several system-level use cases, which motivate the gaps above:

- **Hybrid AC/DC feeders** where LV DC buses support PV, BES, and fast EV charging, while the MV AC side provides feeder-level voltage regulation and power-flow steering (Agrawal et al., 2019; Sun et al., 2022; Qu et al., 2022).
- **Urban resilience and restoration**, where multiple SSTs coordinate to form islands and reconnect, sharing frequency/voltage support and respecting device constraints (Huber & Kolar, 2019; Saleh et al., 2019b).
- Inter-feeder energy exchange without dedicated back-to-back stations, by using SSTs as controllable "power routers" at the feeder boundaries—subject to scalable role assignment and safe primary control (the gaps noted above).
- **Hosting capacity improvements** for DER clusters through volt/var, harmonic mitigation, and fast dynamic regulation distributed at SST nodes (Allende et al., 2020; Shah & Crow, 2016).

5.6 Scope boundary and IP note for this section

The section's technical scope includes coordination of multiple SSTs across feeders, emphasizing role assignment, autonomy during islanding, and communication-free primary control. To keep this report focused on broadly known concepts and to protect pending intellectual property, specific coordination and control strategies developed in this project are intentionally not described here. The literature gaps above are provided to motivate the line of research without disclosing proprietary methods.

6.0 Conclusions and Outlook

This report framed *power-electronics*—enabled grid building blocks as a system-level toolkit and developed two complementary modeling "benches" to exercise them: (i) MT-HVDC with MMC terminals for offshore wind integration, and (ii) MVDC/MV AC hybrid distribution architectures—including SST-based feeders—for controllable transfers and resilience. Throughout, we emphasized architectures, standard control roles, and broadly known operating concepts while intentionally withholding proprietary control designs (now proceeding on separate IP and publication tracks). This approach is consistent with the project's original scope, which called for co-design of PEL building blocks and embedded DC subsystems across architecture, control, and coordination layers.

Deliverables documented in this report:

- MT-HVDC/OWF Use Case platform (EMT): A PSCAD mini-WECC case with five OWF injection points, MMC terminals, and EMT→phasor consistency checks; normal and contingency scenarios demonstrate expected DC-voltage regulation and AC-side behavior under standard droop/slack assignments. The modeling and terminology align with widely used MMC/MTDC practice.
- Two use cases for MVDC coordination:
 - o *IEEE 16-bus MVDC loop* illustrating power scheduling, DC-slack assignment (single-slack vs. distributed droop), and reassignment under contingencies.
 - Olympic Peninsula concept case comparing MV AC vs. MVDC line closures (cost/ROW implications) and steady-state transfer metrics.
- Wind-plant inertial frequency response (IFR): Controlled EMT studies in the 9-bus use case and the 240-bus mini-WECC show (a) baseline and conventional IFR behaviors, (b) risks of aggressive energy extraction (stall/instability if unmanaged), and (c) the system-level value of *smoothed recovery* without disclosing proprietary logic.
- Reusable assets: Parameter tables (cables, distances), MMC models (averaged and switching), E-Tran-based conversion workflow notes, and figure-ready scenarios that illustrate concepts without revealing novel algorithms.

6.1 Evidence of impact and follow-on work (publications/IP)

To keep this public report accessible while protecting novelty, we summarize outcomes at a high level:

- Wind IFR with stall/energy-recovery management. A new IFR framework that actively
 manages available kinetic energy to avoid aerodynamic stalling and excessive recovery has
 progressed to (i) invention disclosure filed with the institution and (ii) externally funded
 follow-on research through DOE's Wind Energy Technologies Office (WETO). A journal
 manuscript based on this line of work has been submitted and is under peer review.
- MVDC role assignment & dual-measurement droop. A control concept for more flexible role assignment in meshed MVDC (including distributed droop/slack scheduling) has been validated in simulation; a journal manuscript is in preparation.
- SST-based autonomous coordination. A communication-free, feeder-level AC coordination strategy for multi-SST islands has been demonstrated in simulation (with PV/BES on each feeder and stable interaction with upstream wind support). A journal manuscript is in preparation.

Conclusions and Outlook 41

- SST-enabled MVDC meshing across feeders. A concept to form meshed MVDC using feeder-level SSTs (beyond single-device microgrid use) is in preparation for journal submission.
- Olympic Peninsula MVDC study. A conference paper on steady-state performance and cost/ROW tradeoffs for MVDC closure around the peninsula is in progress.

6.2 Key technical lessons

- 1. EMT-level fidelity is often necessary to faithfully capture interactions among MMCs, IBRs, and weak-area dynamics; phasor checks remain useful for the electromechanical band.
- 2. In IFR, the *recovery phase* is at least as critical as the initial energy release; unmanaged recovery can precipitate stall and instability.
- 3. In meshed MVDC, there is no single universal rule for slack/droop assignment; flexible role scheduling improves utilization and contingency response but must be introduced without compromising the opposite-side control mode.
- 4. At distribution scale, SSTs should be treated as *architectural nodes*—not merely conversion devices—so that feeder-level coordination (and island formation) is designed from the outset. These themes are consistent with established MMC/MTDC foundations and emerging practice.

Team roles are summarized below using the CRediT taxonomy:

The PI, Hisham Mahmood, provided technical leadership and integration across Sections 2–5 (conceptualization, methodology, modeling, validation, analysis, writing, supervision), developing and testing the novel control concepts whose details are reserved for publications and IP review. Buxin She developed the mini-WECC EMT base case and supported E-Tran transfer and validation. Gian Paramo performed the MVDC-vs-AC cost and right-of-way (ROW) analysis for the Olympic Peninsula use case, prepared the associated figures, and authored the cost-analysis section of the conference paper draft. Roshan L. Kini and Priya T. Mana contributed literature review and data curation for Section 2 and parameterized the WSCC 9-bus Simulink model. Marcelo A. Elizondo served as thrust lead, providing supervision, program alignment, and milestone oversight.

Scope boundary

Protection systems (AC/DC fault detection/clearing), detailed vendor-specific implementations, and the exact logic of the new control designs are **out of scope** for this public report. Where results could reveal unpublished ideas, we restricted ourselves to standard behaviors, safe scenarios, and descriptive figures. The full control formulations will appear in the cited manuscripts and/or patent filings after appropriate review.

Conclusions and Outlook 42

7.0 References

- A. Agrawal, C. S. Nalamati, and R. Gupta, "Hybrid DC–AC Zonal Microgrid Enabled by Solid-State Transformer and Centralized ESD Integration," *IEEE Transactions on Industrial Electronics*, vol. 66, no. 11, pp. 9097–9107, 2019. doi:10.1109/TIE.2019.2899559. (Agrawal et al., 2019)
- J. Aho, A. Buckspan, J. Laks, P. Fleming, Y. Jeong, F. Dunne, M. Churchfield, L. Pao, and K. Johnson, "A Tutorial of Wind Turbine Control for Supporting Grid Frequency through Active Power Control," in *Proc. American Control Conf.*, Montreal, 2012. (Aho et al., 2012)
- S. W. Ali et al., "Offshore Wind Farm–Grid Integration: A Review on Infrastructure, Challenges, and Grid Solutions," *IEEE Access*, vol. 9, pp. 102811–102825, 2021. (Ali et al., 2021)
- F. R. Allende, M. A. Perez, J. R. Espinosa, T. Gajowik, S. Stynski, and M. Malinowski, "Surveying Solid-State Transformer Structures and Controls: Providing Highly Efficient and Controllable Power Flow in Distribution Grids," *IEEE Industrial Electronics Magazine*, vol. 14, no. 1, pp. 56–70, 2020. doi:10.1109/MIE.2019.2950436. (Allende et al., 2020)
- D. Cervero, M. Fotopoulou, J. Muñoz-Cruzado, D. Rakopoulos, F. Stergiopoulos, N. Nikolopoulos, S. Voutetakis, and J. F. Sanz, "Solid State Transformers: A Critical Review of Projects with Relevant Prototypes and Demonstrators," *Electronics*, vol. 12, no. 4, Article 931, 2023. Available: https://www.mdpi.com/2079-9292/12/4/931. (Cervero et al., 2023)
- C.-J. Chou, Y.-K. Wu, G.-Y. Han, and C.-Y. Lee, "Comparative Evaluation of the HVDC and HVAC Links Integrated in a Large Offshore Wind Farm—An Actual Case Study in Taiwan," *IEEE Transactions on Industry Applications*, vol. 48, no. 2, 2012. (Chou et al., 2012)
- Y. Cui, X. He, X. Yang, W. Wang, L. Cao, and M. Jin, "Electromechanical–Electromagnetic Hybrid Simulation Based on E-Tran Plus," *IOP Conf. Ser.: Materials Science and Engineering*, vol. 563, 052103, 2019. https://doi.org/10.1088/1757-899X/563/5/052103. (Cui et al., 2019)
- Das, Dwijasish; Hrishikesan, V. M.; Kumar, Chandan; Liserre, Marco. "Smart Transformer-Enabled Meshed Hybrid Distribution Grid." *IEEE Transactions on Industrial Electronics*, 68(1), 282–292, 2021. doi:10.1109/TIE.2020.2965489. (Das et al., 2021)
- Das, Dwijasish; Manojkumar, Rampelli; Kumar, Chandan; Ganguly, Sanjib. "Power Loss Minimization in Smart Transformer Enabled Low Voltage Islanded Meshed Hybrid Microgrid." *IEEE Access*, 10, 123259–123270, 2022. doi:10.1109/ACCESS.2022.3224001. (Das et al., 2022)
- Das, Dwijasish; Kumar, Chandan; Liserre, Marco. "Stabilization of Smart Transformer Based Islanded Meshed Hybrid Microgrid During Electric Vehicle Charging Transients." *IEEE Journal of Emerging and Selected Topics in Industrial Electronics*, 4(4), 1255–1264, 2023. doi:10.1109/JESTIE.2023.3294088. (Das et al., 2023)
- R. G. de Almeida and J. P. Lopes, "Participation of Doubly Fed Induction Wind Generators in System Frequency Regulation," *IEEE Transactions on Power Systems*, vol. 22, no. 3, pp. 944–950, Aug. 2007. doi:10.1109/TPWRS.2007.901096. (de Almeida & Lopes, 2007)

- U.S. DOE Office of Electricity, Transformer Resilience and Advanced Components (TRAC) Program, *Solid State Power Substation Technology Roadmap*, Jul. 2020. Available: https://www.energy.gov/oe/articles/oe-report-solid-state-power-substation-technology-roadmap. (DOE TRAC, 2020)
- T. C. Douville et al., "Capacity Contributions of Southern Oregon Offshore Wind to ...," 2024. (Douville et al., 2024)

Electranix, "E-TRAN / E-TRAN Plus for PSCAD—Software Description and Application Notes," Electranix product documentation.

L. Fan, "Wind in Weak Grids: 4 Hz or 30 Hz Oscillations?," 2018.

GE Energy Consulting (N. Miller, D. Lew, R. Piwko, et al.), *Technology Capabilities for Fast Frequency Response (AEMO Future Power System Security Program)*, Mar. 9, 2017. (GE Energy Consulting, 2017)

Ge, Junjie; Zhao, Zhengming; Yuan, Liqiang; Lu, Ting. "Energy Feed-Forward and Direct Feed-Forward Control for Solid-State Transformer." *IEEE Transactions on Power Electronics*, **30**(8): 4042–4047, 2015. doi:10.1109/TPEL.2014.2382613. (Ge et al., 2015)

- P. A. Gray, Z. C. Ma, and P. W. Lehn, "A High-Frequency MMC for DC–DC Applications Using a Three-Winding Transformer with DC Flux Cancellation," *IEEE Journal of Emerging and Selected Topics in Industrial Electronics*, vol. 3, no. 3, pp. 647–657, 2022. doi:10.1109/JESTIE.2021.3116512. (Gray et al., 2022)
- J. E. Huber and J. W. Kolar, "Applicability of Solid-State Transformers in Today's and Future Distribution Grids," *IEEE Transactions on Smart Grid*, vol. 10, no. 1, pp. 317–326, 2019. doi:10.1109/TSG.2017.2738610. (Huber & Kolar, 2019)

CIRED Working Group 2019-1, DC Distribution Networks—Final Report, 2021.

KIOS Centre for Intelligent Systems & Networks, *IEEE 9-Bus Modified Test System*, 2013. (KIOS, 2013)

- F. Li, J. Zhu, L. Yu, S. Bu, H. Zhao, J. Zhao, Y. Xu, J. M. Guerrero, and C. Wang, "An Imbalance-Status-Enabled Autonomous Global Power-Sharing Scheme for Solid-State Transformer Interconnected Hybrid AC/DC Microgrids," *IEEE Transactions on Smart Grid*, vol. 14, no. 3, pp. 1750–1762, 2023. doi:10.1109/TSG.2022.3216853. (Li et al., 2023)
- Y. Liao, H. Wu, X. Wang, M. Ndreko, R. Dimitrovski, and W. Winter, "Stability and Sensitivity Analysis of Multi-Vendor, Multi-Terminal HVDC Systems," *IEEE Open Journal of Power Electronics*, 2023. (Liao et al., 2023)
- S. P. Martin, X. Dong, and H. Li, "Model Development and Predictive Control of a Low-Inertia DC Solid-State Transformer (SST)," *IEEE Journal of Emerging and Selected Topics in Power Electronics*, vol. 10, no. 6, pp. 6482–6494, 2022. doi:10.1109/JESTPE.2022.3159621. (Martin et al., 2022)

NERC Inverter-Based Resource Performance Task Force (IRPTF), Fast Frequency Response Concepts and Bulk Power System Reliability Needs, White Paper, Mar. 2020. (NERC, 2020)

- North American Electric Reliability Corporation, *Frequency Response Initiative Report (with Appendices)*, Oct. 2012. (NERC, 2012)
- J. Nie, L. Yuan, W. Wen, R. Duan, B. Shi, and Z. Zhao, "Communication-Independent Power Balance Control for Solid State Transformer Interfaced Multiple Power Conversion Systems," *IEEE Transactions on Power Electronics*, vol. 35, no. 4, pp. 4256–4271, 2020. doi:10.1109/TPEL.2019.2936109. (Nie et al., 2020)
- PSCAD, *PRSIM™ User Manual / Tutorial (v1.1.0)*, 2023. (PSCAD, 2023)
- J. Price and J. Goodin, "Reduced Network Modeling of WECC as a Market Design Prototype," in *Proc. IEEE PES General Meeting*, 2011. (Price & Goodin, 2011)
- Z. Qu, Z. Shi, Y. Wang, A. Abu-Siada, Z. Chong, and H. Dong, "Energy Management Strategy of AC/DC Hybrid Microgrid Based on Solid-State Transformer," *IEEE Access*, vol. 10, pp. 20633–20642, 2022. doi:10.1109/ACCESS.2022.3149522. (Qu et al., 2022)
- M. A. Rahman, M. R. Islam, K. M. Muttaqi, and D. Sutanto, "Data-Driven Coordinated Control of Converters in a Smart Solid-State Transformer for Reliable and Automated Distribution Grids," *IEEE Transactions on Industry Applications*, vol. 56, no. 4, pp. 4532–4542, 2020. doi:10.1109/TIA.2020.2972507. (Rahman et al., 2020)
- L. Ren, L. Zhang, H. Guo, C. Xu, F. Wang, M. Zhou, T. Shi, D. Gong, and D. Du, "Distributed Power Management and Adaptive Coordinated Control for SST-Based Power Systems," *IEEE Transactions on Industry Applications*, vol. 59, no. 5, pp. 6457–6467, 2023. doi:10.1109/TIA.2023.3275554. (Ren et al., 2023)
- S. A. M. Saleh, C. Richard, X. F. St. Onge, K. M. McDonald, E. Ozkop, and L. Chang, "Solid-State Transformers for Distribution Systems—Part I: Technology and Construction," *IEEE Transactions on Industry Applications*, vol. 55, no. 5, pp. 4524–4535, 2019. doi:10.1109/TIA.2019.2923163. (Saleh et al., 2019a)
- S. A. M. Saleh, E. Ozkop, B. Alsayid, C. Richard, X. F. St. Onge, K. M. McDonald, and L. Chang, "Solid-State Transformers for Distribution Systems—Part II: Deployment Challenges," *IEEE Transactions on Industry Applications*, vol. 55, no. 6, pp. 5708–5716, 2019. doi:10.1109/TIA.2019.2938143. (Saleh et al., 2019b)
- D. Shah and M. L. Crow, "Online Volt–Var Control for Distribution Systems With Solid-State Transformers," *IEEE Transactions on Power Delivery*, vol. 31, no. 1, pp. 343–350, 2016. doi:10.1109/TPWRD.2015.2457442. (Shah & Crow, 2016)
- K. Sharifabadi, L. Harnefors, H.-P. Nee, S. Norrga, and R. Teodorescu, *Design, Control, and Application of Modular Multilevel Converters for HVDC Transmission Systems*. Wiley, 2016. (Sharifabadi et al., 2016)
- B. She, H. Mahmood, M. Elizondo, V. Adetola, and Y. Dong, "Configuration and EMT Simulation of the 240-Bus MiniWECC System Integrating Offshore Wind Farms (OWFs)," arXiv:2403.07988, 2024. (She et al., 2024)

Siemens Energy, MVDC PLUS® product overview/white paper, 2024. (Siemens Energy, 2024)

- Y. Sun, Z. Gao, C. Fu, C. Wu, and Z. Chen, "A Hybrid Modular DC Solid-State Transformer Combining High Efficiency and Control Flexibility," *IEEE Transactions on Power Electronics*, vol. 35, no. 4, pp. 3434–3449, 2020. doi:10.1109/TPEL.2019.2935029. (Sun et al., 2020)
- Q. Sun, Y. Li, D. Ma, Y. Zhang, and D. Qin, "Model Predictive Direct Power Control of a Three-Port Solid-State Transformer for Hybrid AC/DC Zonal Microgrid Applications," *IEEE Transactions on Power Delivery*, vol. 37, no. 1, pp. 528–538, 2022. doi:10.1109/TPWRD.2021.3064418. (Sun et al., 2022)
- D. Van Hertem, O. Gomis-Bellmunt, and J. Liang, *HVDC Grids: For Offshore and Supergrid of the Future*. Wiley-IEEE Press, 2016. (Van Hertem et al., 2016)
- K. V. Vidyanandan and N. Senroy, "Primary Frequency Regulation by Deloaded Wind Turbines Using Variable Droop," *IEEE Transactions on Power Systems*, vol. 28, no. 2, pp. 837–846, May 2013. doi:10.1109/TPWRS.2012.2216879. (Vidyanandan & Senroy, 2013)
- H. V. M. and C. Kumar, "Operation of Meshed Hybrid Microgrid During Adverse Grid Conditions With Storage Integrated Smart Transformer," *IEEE Open Journal of the Industrial Electronics Society*, vol. 2, pp. 315–325, 2021. doi:10.1109/OJIES.2021.3073142. (Hrishikesan & Kumar, 2021)
- V. M. Hrishikesan, C. Kumar, and M. Liserre, "An MVDC-Based Meshed Hybrid Microgrid Enabled Using Smart Transformers," *IEEE Transactions on Industrial Electronics*, vol. 69, no. 4, pp. 3722–3731, 2022. doi:10.1109/TIE.2021.3071683. (Hrishikesan et al., 2022)
- V. M. Hrishikesan and C. Kumar, "Smart Transformer-Based Meshed Hybrid Microgrid with MVDC Interconnection," in *Proc. IECON 2020—46th Annual Conf. IEEE Industrial Electronics Society*, 2020, pp. 4961–4966. doi:10.1109/IECON43393.2020.9255284. (Hrishikesan & Kumar, 2020)
- F. Wald, Q. Tao, and G. De Carne, "Virtual Synchronous Machine Control for Asynchronous Grid Connections," *IEEE Transactions on Power Delivery*, vol. 39, no. 1, pp. 397–406, 2024. doi:10.1109/TPWRD.2023.3235149. (Wald et al., 2024)
- B. Wang et al., *Developing a PSCAD Model of the Reduced 240-Bus WECC System*, NREL/TP-5D00-82287, 2022. (Wang et al., 2022)
- X. Yu, X. She, X. Ni, and A. Q. Huang, "System Integration and Hierarchical Power Management Strategy for a Solid-State Transformer Interfaced Microgrid System," *IEEE Transactions on Power Electronics*, vol. 29, no. 8, pp. 4414–4425, 2014. doi:10.1109/TPEL.2013.2289374. (Yu et al., 2014)
- CIGRE JWG C6/B4.37, *Medium Voltage DC Distribution Systems*, Technical Brochure 875, 2022. (Yu et al., 2022)
- H. Yuan, Developing a Reduced 240-Bus WECC Dynamic Model for Frequency Response Study of High Renewable Integration, NREL preprint, 2020 (later conf. versions 2021/2022). (Yuan, 2020)

H. Zong, J. Lyu, X. Wang, C. Zhang, R. Zhang, and X. Cai, "Grey-Box Aggregation Modeling of Wind Farm for Wideband Oscillations Analysis," *Applied Energy*, vol. 283, 116035, 2021. https://doi.org/10.1016/j.apenergy.2020.116035. (Zong et al., 2021)

Pacific Northwest National Laboratory

902 Battelle Boulevard P.O. Box 999 Richland, WA 99354

1-888-375-PNNL (7665)

www.pnnl.gov